DEVELOPMENT OF A THREE-DIMENSIONAL FLUX SYNTHESIS PROGRAM AND COMPARISON WITH 3-D TRANSPORT THEORY RESULTS

A Thesis

Submitted to the Graduate Faculty of the
Louisiana State University and
Agricultural and Mechanical College
in partial fulfillment of the
requirements for the degree of
Master of Science in Nuclear Engineering
in
The Department of Nuclear Engineering

by
Prosanta Chowdhury
M.S., Moscow Power Engineering Institute, 1982
May 1987

ACKNOWLEDGEMENTS

The author is deeply indebted to his major professor Dr. Mark L. Williams, associate professor of the LSU Nuclear Science Center, who provided and has been providing invaluable technical assistance, suggestions and encouragement throughout the entire period of study.

The author is grateful to the Engineering Physics and the Operations Divisions of Oak Ridge National Laboratory (ORNL), Oak Ridge, Tennessee, for funding this study. F. B. K. Kam of the Operations Division was especially helpful and provided funding for this project beyond the original estimated amount. Funds were provided by the U.S. Nuclear Regulatory Commission for validation studies and by the Electric Power Research Institute for code development. W. A. Rhoades and R. L. Childs are thanked for permitting use of the Three-Dimensional Oak Ridge Transport Code "TORT", which they developed.

The author expresses his gratitude to the LSU faculty Dr. John C. Courtney, professor of Nuclear Engineering, Dr. Adnan Yücel, assistant professor of Nuclear Engineering, and Dr. Gill G. Richards, associate professor of Electrical Engineering for kindly reviewing the thesis work.

The author also acknowledges his indebtedness to Dr. Frank F. Iddings, former assistant director, LSU Nuclear Science Center, who helped the author to enroll in the LSU Nuclear Engineering Program.

Mr. Richard E. Teague of the Nuclear Science Center extended help in solving numerous computer programming problems. Mrs. Yvonne Thomas of the Nuclear Science Center has helped while preparing the draft of the thesis, and Mrs. Brenda Taylor of the ORNL Operations Division prepared the final copy. The author is thankful to each of them.

Finally, the author is grateful to his wife for her help, suggestions and encouragement during this study.

TABLE OF CONTENTS

TABLE OF CONTENTS (Continued)

LIST OF TABLES

LIST OF FIGURES

LIST OF FIGURES (Continued)

ABSTRACT

A three-dimensional flux synthesis program called DOTSYN is developed to estimate neutron fluence in light water reactors (LWRs). The main purpose of developing this program is to provide the U.S. utilities with an economical tool for routine three-dimensional fluence calculations at various ex-core locations in a reactor, especially at critical pressure vessel sites for embrittlement analysis. The synthesis is based on a simple expression which uses lower dimensional flux values obtained from 2-D and 1-D transport theory calculations to approximate the desired 3-D fluxes. In order to verify the accuracy and efficiency of the method, a simulated PWR, similar in configuration to the Babcock and Wilcox Arkansas Nuclear One Unit 1 (ANO-1) reactor, is modeled in three-dimensional cylindrical coordinates, and calculations are performed with the Three-dimensional Oak Ridge Transport code TORT as well as with DOTSYN. Results by TORT are used as a reference three-dimensional "benchmark" solution, and DOTSYN results at various locations, especially near the pressure vessel, are compared to this reference solution. The error between TORT and DOTSYN results at the peak flux locations (θ = 9°) at the inner surface of the pressure vessel varies between 0.36% at the midplane and 4.73% at the bottom of the nozzle. The worst agreement was found to be about 19.8% at the bottom of the nozzle at an azimuth of about 39.5°. The above calculations are performed for five energy groups for which the TORT calculation required about five CPU hours (on an IBM 3033 computer) whereas DOTSYN along with three DOT-IV (2-D discrete ordinates transport code) runs took only about eight minutes of CPU time.

It is concluded that the 3-D synthesis method is a very efficient method for estimating reactor pressure vessel fluence, which gives acceptable accuracy even at axial locations far above the active core height.

CHAPTER I

INTRODUCTION

Estimation of the neutron flux at various locations in the reactor pressure vessels (RPVs) of light water reactors (LWRs) is extremely important for safety as well as economic considerations. The U.S. Nuclear Regulatory Commission (NRC) requires that each nuclear reactor maintain an RPV surveillance program to ensure that the vessel fluence does not exceed a maximum allowable value. This is necessary because bombardment of the RPV by high-energy neutrons will eventually cause embrittlement of the steel vessel, which could result in vessel failure under certain accident conditions which place the RPV under thermal stress.

There are two general locations in the RPV where possibilities of embrittlement must be estimated[1]:

(i) somewhere near the 1/4th thickness along the reactor horizontal midplane; and

(ii) at the inner surface for critical weld locations above or below the active fuel height.

The first of the locations is close to the point where fluence is maximum. This location is important for reactor lifetime considerations. At the second location the fluence is less, but the thermal stress can be much higher during transients such as encountered when the inlet water temperature is rapidly decreased; and, depending on the composition of the weld material, the degree of embrittlement may be higher. If the RPV

fluence is large enough that the steel has become very brittle, then the second location is susceptible to fracture during sudden emergency coolant flow and subsequent repressurization during a loss-of-coolant accident - this phenomenon is called "Pressurized Thermal Shock (PTS)"[1].

The determination of the RPV fluence is a complex procedure. The most accurate method to determine RPV fluence is to combine the results of neutron transport calculations with surveillance dosimetry measurements[1]. The dosimeter measurements are performed by measuring the activities of various irradiated foils composed of materials having high-energy threshold reactions. These activities provide a direct experimental estimate for the flux. Unfortunately, the dosimeter data are rather limited; they only provide information at a few points within the reactor, and do not provide sufficient data concerning the energy distribution of the neutrons striking the vessel, which is important in assessing the radiation damage to the RPV. Thus, it is necessary to supplement the dosimetry analysis with transport calculations. The accuracy of the transport calculations can be verified by comparing the computed versus measured dosimeter activities at the surveillance locations.

In the transport calculations, a calculational model is necessary which can predict at any stage in reactor life the detailed three-dimensional (3-D), energy-dependent RPV flux distribution as well as the computed estimates for the surveillance dosimeter activities, since the incident RPV flux varies in all three spatial dimensions.

A finite difference numerical calculation with a detailed 3-D mesh would be the apparent method for this purpose[2]. Unfortunately, until very recently no such codes had been developed. The DOT-IV computer code

[developed in Oak Ridge National Laboratory (ORNL), Oak Ridge, Tennessee] has been extensively used for transport theory calculations of reactor shields; however, it cannot treat 3-D geometry explicitly. Rather, it calculates fluxes for two-dimensional (2-D) geometries (namely, X-Y, R-Z, R-θ) and one-dimensional (1-D) geometries (X, R). Recently at ORNL, a new computer code called TORT has been developed for solving the 3-D transport equation, but it has not been released to the public. Using a 3-D code of this type for the purpose of RPV fluence determination is very expensive, and not practical for routine utility applications. Furthermore, in many regions important for RPV safety analysis, the core power varies slowly in the axial dimension and the shape is rather uniform. Therefore, utilities do not really need a detailed 3-D calculational model. If by some means, we could avoid performing 3-D transport calculations by using some other methods that yield a good approximation to the true 3-D flux distribution, much computer time could be saved and the cost of calculations could be reduced dramatically.

Much effort has been made in the past to develop methods of constructing a 3-D flux shape by combining the results of 1-D and 2-D calculations[2]. The procedure of constructing a 3-D solution from the combination of lower dimensional calculations is called "Synthesis", and the resulting approximate fluxes are referred to as "Synthesized Fluxes". The vast majority of synthesis studies have focused on obtaining a 3-D representation of the power distribution within the reactor core, and were usually based on the diffusion theory approximation to the transport equation.

Although diffusion theory cannot be used accurately for the determination of the RPV fluence, it is instructive to consider a simple

synthesis example based on diffusion theory. The solution to a rectangular, parallelopiped reactor with no axial variation of materials properties (i.e., a truly separable problem) is a simple example of synthesized flux:

$$\Psi_g(x,y,z) = \text{Cos}(B_z z)H_g(x,y) \quad (1)$$

where, $H_g(x,y)$ is the solution of the 2-D problem in the x,y plane with a transverse buckling of $B_z{}^2$; and "g" is the energy group index. Here, the synthesized and exact solutions are identical because the axial variation for the flux is the same at all (x,y) points. This is true for any truly separable problem[2].

The so-called "Conventional" synthesis method has been widely used in reactor physics calculations for axially non-uniform reactors, having a small number of axial zones. This approach essentially assumes that the flux is separable in each axial zone. For example, a reactor having two axial zones separated by a control rod bank has the following approximate solution by the conventional method:

$$\Psi_g(x,y,z) = Z_g(z) \begin{cases} H_{1g}(x,y), & 0<z\leq z_R \\ H_{2g}(x,y), & z_R<z\leq L \end{cases} \quad (2)$$

where, H_{1g} and H_{2g} are the solutions of 2-D problems with rods out and rods in, respectively, and with the axial buckling chosen to be consistent with the subsequently determined $Z_g(z)$; z_R is the height of the first zone and $(L-z_R)$ is the height of the second zone[2]. Although this method is easy to use, the synthesized flux shapes with this method have discontinuities at the axial zone interfaces.

Several other synthesis techniques which may improve upon the conventional method have been suggested to approximate 3-D fluxes. For the diffusion equation, the following methods are used for synthesis[2,3]: (1) weighted-residual method; (2) variational methods; (3) multichannel synthesis; and (4) method based on gross coupling. These methods were developed mainly for in-core reactor physics calculations, and have not been used for ex-core, deep penetration problems, such as encountered in flux calculations near the RPV.

In order to apply a synthesis approximation to RPV fluence prediction, it is necessary to develop a method which is applicable to ex-core calculations based on the transport theory. The primary objectives of this study are:

(a) to develop a synthesis code (to be called DOTSYN) which performs 3-D synthesis of 2-D and 1-D fluxes computed by DOT-IV. This program is to be provided to the Electric Power Research Institute (EPRI) for distribution to U.S. utilities as part of the LEPRICON (Least-Squares EPRI Consolidation) computer code system for RPV fluence determination;

(b) to model a typical PWR reactor configuration in three dimensions and perform 3-D discrete ordinates transport calculations with the 3-D transport code TORT;

(c) to perform R-θ, R-Z, and 1-D (R) calculations with DOT-IV for the same configuration;

(d) to use results of DOT-IV R-θ, R-Z, and 1-D (R) calculations to synthesize a 3-D flux distribution with DOTSYN; and

(e) to compare the results obtained from the 3-D TORT calculations and the DOTSYN synthesis in order to verify the accuracy of the proposed synthesis method.

CHAPTER II

THEORETICAL BACKGROUND

A. Steady State Transport Equation in Multigroup Form

By definition, a steady state condition is one in which the rate of neutron loss in $dEd\hat{\Omega}dV$ equals the rate of gain or production, where dE, $d\hat{\Omega}$, dV are differential energy, direction and volume elements, respectively. If we express this differential neutron balance condition (loss = production) in terms of the angular neutron flux $\Psi(\mathbf{r},E,\hat{\Omega})$ which depends on space, energy and direction coordinates, then we obtain a mathematical expression called the Boltzman Transport Equation for the directional flux density $\Psi(\mathbf{r},E,\hat{\Omega})$.

There exist several forms of the transport equation, namely,

1. integrodifferential form;
2. integral form; and
3. surface-integral form.

The direct integration method has been applied to solve the neutron transport equation in X-Y-Z geometry.[4]

In this study, the integrodifferential form of the transport equation is used in R-Θ-Z and we shall deal with only one of the methods of solution applied to this form, namely, the discrete ordinates technique which is most often used in RPV fluence analysis.

In three dimensions, the multigroup form of the integrodifferential transport equation for energy group "g" can be written as follows

$$\nabla\cdot\hat{\Omega}\Psi_g + \Sigma_{Tg}\Psi_g = \sum_{g'}\int_{\Omega'}\Sigma_{sg'\to g}(\hat{\Omega}'\to\hat{\Omega})\Psi_{g'}d\hat{\Omega}' + Q_g \quad \text{- - - - - - - - - - - - -} \quad (3)$$

where, $\Psi_g \equiv$ multigroup angular neutron flux which is a function of six independent variables that define the neutron position ($\vec{r}$), direction of propagation ($\hat{\Omega}$), and energy group (g);

$\Sigma_{Tg} \equiv$ total cross section (XS) for group "g";

$\Sigma_{sg'\to g}(\hat{\Omega}'\to\hat{\Omega}) \equiv$ angle-dependent (differential) scatter XS for a neutron in energy group g', traveling in a direction $\hat{\Omega}'$ to scatter to energy group g in the direction $\hat{\Omega}$;

$Q_g \equiv$ source of neutrons (fission and external);

$\hat{\Omega} \equiv$ neutron direction defined by the direction cosines $(\mu, \eta, \xi) = \left(\mu, \eta, \sqrt{1-\mu^2-\eta^2}\right)$.

An R-θ-Z cylindrical model of the reactor is used for most RPV flux calculations, where R, θ, and Z are the radial, azimuthal, and axial coordinates, respectively (fig. 1). Equation (3) can be written in R, θ, Z, system of coordinates as follows

$$\frac{\mu}{R}\frac{\partial(R\Psi_g)}{\partial R} + \frac{\eta}{R}\frac{\partial\Psi_g}{\partial\theta} + \xi\frac{\partial\Psi_g}{\partial Z} - \frac{1}{R}\frac{\partial(\eta\Psi_g)}{\partial\omega} + \Sigma_{Tg}\Psi_g = \sum_{g'}\int_{\hat{\Omega}'}\Sigma_{sg'\to g}(\hat{\Omega}'\to\hat{\Omega})\Psi_{g'}d\hat{\Omega}' + Q_g \quad (4)$$

where, μ, η, ξ are the direction cosines of $\hat{\Omega}$ in the R, θ, Z directions, respectively. Often transport calculations are performed for lower dimensional sub-spaces of the 3-D R-θ-Z space. Of interest in this study are the following sub-spaces:

(a) R-θ geometry (2-D), which corresponds to a slice through an infinitely tall cylinder. The flux varies radially and azimuthally, but is constant axially.

(b) R-Z geometry (2-D), which corresponds to a finite height

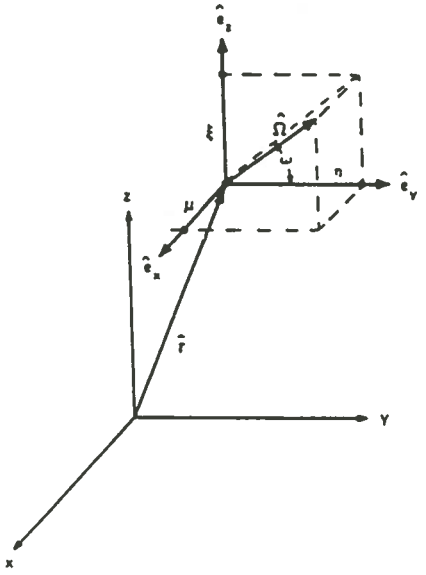

(i)

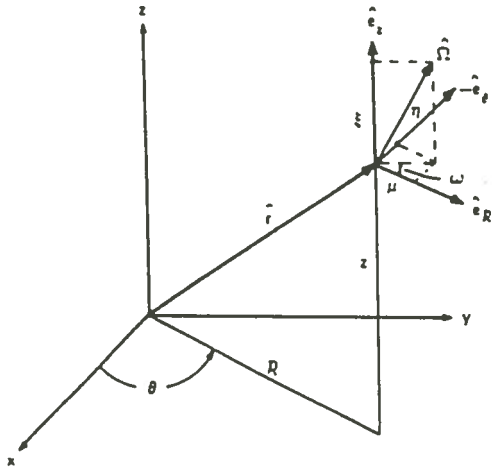

(ii)

Fig. 1. (i) Cartesian space-angle coordinate system in three dimensions.
(ii) Cylindrical space-angle coordinate system in three dimensions

cylinder which is azimuthally uniform. The flux varies radially and axially, but is constant azimuthally.

(c) R geometry (1-D), which corresponds to an infinitely tall, azimuthally uniform cylinder. The flux varies only in the radial direction.

In 2-D R-θ coordinates, equation (4) reduces to

$$\frac{\mu}{R}\frac{\partial(R\Psi_g)}{\partial R} + \frac{\eta}{R}\frac{\partial\Psi_g}{\partial\theta} - \frac{1}{R}\frac{\partial(\eta\Psi_g)}{\partial\omega} + \Sigma_{Tg}\Psi_g$$

$$= \sum_{g'}\int_{\hat{\Omega}'}\Sigma_{sg'\to g}(\hat{\Omega}'\to\hat{\Omega})\Psi_{g'}d\hat{\Omega}' + Q_g \quad \text{- - - - - - - - - - - - - - - - - (5)}$$

In 2-D R-Z, equation (4) has the following form:

$$\frac{\mu}{R}\frac{\partial(R\Psi_g)}{\partial R} + \xi\frac{\partial\Psi_g}{\partial Z} - \frac{1}{R}\frac{\partial(\eta\Psi_g)}{\partial\omega} + \Sigma_{Tg}\Psi_g$$

$$= \sum_{g'}\int_{\hat{\Omega}'}\Sigma_{sg'\to g}(\hat{\Omega}'\to\hat{\Omega})\Psi_{g'}d\hat{\Omega}' + Q_g \quad \text{- - - - - - - - - - - - - - - - - (6)}$$

In 1-D (R) cylindrical geometry, equation (4) is written as

$$\frac{\mu}{R}\frac{\partial(R\Psi_g)}{\partial R} - \frac{1}{R}\frac{\partial(\eta\Psi_g)}{\partial\omega} + \Sigma_{Tg}\Psi_g$$

$$= \sum_{g'}\int_{\hat{\Omega}'}\Sigma_{sg'\to g}(\hat{\Omega}'\to\hat{\Omega})\Psi_{g'}d\hat{\Omega}' + Q_g \quad \text{- - - - - - - - - - - - - - - - - (7)}$$

B. The Discrete Ordinates Method

The continuous Boltzman Transport Equation is expressed in terms of discrete variables by the discrete ordinates method. The differential intervals dE, $d\hat{\Omega}$, dV over which the transport equation expresses a particle balance are represented by finite intervals ΔE_g, $\Delta\hat{\Omega}_m$, ΔV_i. The discrete ordinates equation thus expresses a particle balance over these finite-sized intervals.

In the discrete ordinates approximation, a numerical quadrature in the angular variable is used to evaluate the integral appearing in the transport equation; i.e., a finite set of N angular directions $\hat{\Omega}_m$ and associated weights W_m, specified on a unit sphere of directions, is used to define a quadrature formula[5]. As a result of this, a system of N coupled ordinary differential equations emerges, which describe the angular fluxes in the directions specified by the quadrature formula; in other words, the integrodifferential form of the transport equation is replaced by a purely differential form with the integral term expressed as a quadrature summation. These equations are solved by a finite difference technique. In treating the spatial variable, the domain is decomposed into a set of discrete homogeneous cells by defining a spatial mesh. For a given direction $\hat{\Omega}_m$ a finite number of flux values, representing cell-averaged fluxes, describe the angular fluxes $\Psi_m(\mathbf{r})$ within the spatial domain. The energy group boundaries provide energy discretization.

1. Angular Discretization

Two angular coordinates are required to specify the direction of neutron travel ($\hat{\Omega}$) in multidimensional problems. As will be shown

later, these two angles are specified in a local system of coordinates relative to an orthogonal system of coordinates (fig. 1a). The unit vector $\hat{\Omega}$ defines a point on the surface of a unit sphere which is mapped out by all possible directions of neutron travel. In 2-D problems, due to symmetry conditions, the angular flux is calculated over only four of the octants of the unit sphere described by the unit direction vector $\hat{\Omega}$. In 3-D problems, the angular flux must be determined over all eight octants.

In the discrete ordinates method, each of the N discrete directions intersects the surface of the unit sphere at a particular point, and the whole surface of this unit sphere is considered to be divided into N surface elements which contain these points. A point of intersection can be thought to be located at the center of a solid angle "direction interval" (fig. 2).

Each discrete direction $\hat{\Omega}_m$ (m = 1,N) is associated with an area element ΔA_m which is proportional to the solid angle interval $\Delta\hat{\Omega}_m$ (in steradians) about $\hat{\Omega}_m$, i.e.,

$$\Delta A_m = \Delta\hat{\Omega}_m * \rho^2 \quad - - - - - - - - - - - - - - - - - - \quad (8)$$

The magnitudes of the direction intervals ($\Delta\hat{\Omega}_m$) are called the quadrature weights. The weights are generally normalized to unity in discrete ordinates calculations, so that:

$$W_m = \frac{\Delta A_m}{4\pi\rho^2} = \frac{\Delta A_m}{4\pi} \quad - - - - - - - - - - - - - - - - - \quad (8a)$$

Figure 3 shows a level symmetric quadrature where the ordinates are arranged on the unit octant; these types of quadratures are widely used and they utilize the same set of N/2 positive values of the direction

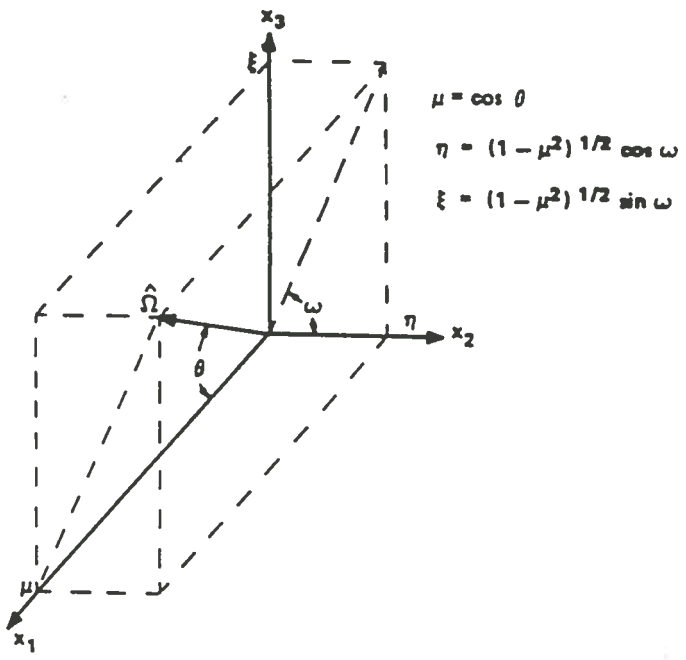

Fig. 1a. Angular coordinate system

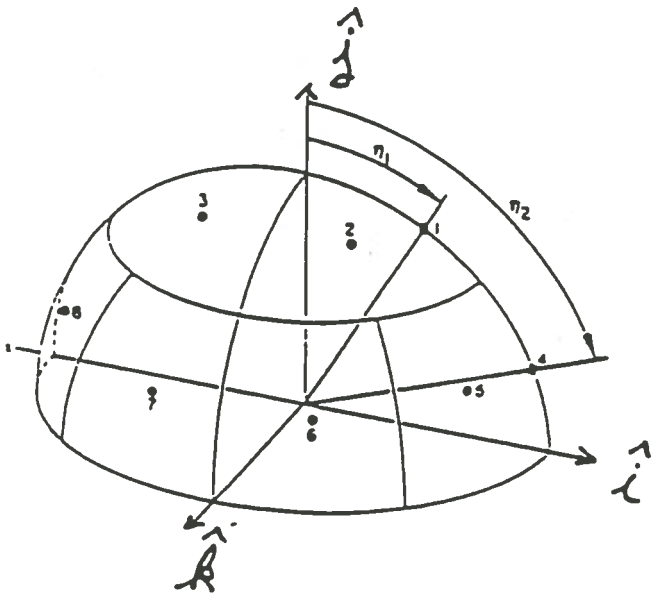

Fig. 2. Division of a unit sphere into "directional mesh" (only upper section for S_4 quadrature shown)

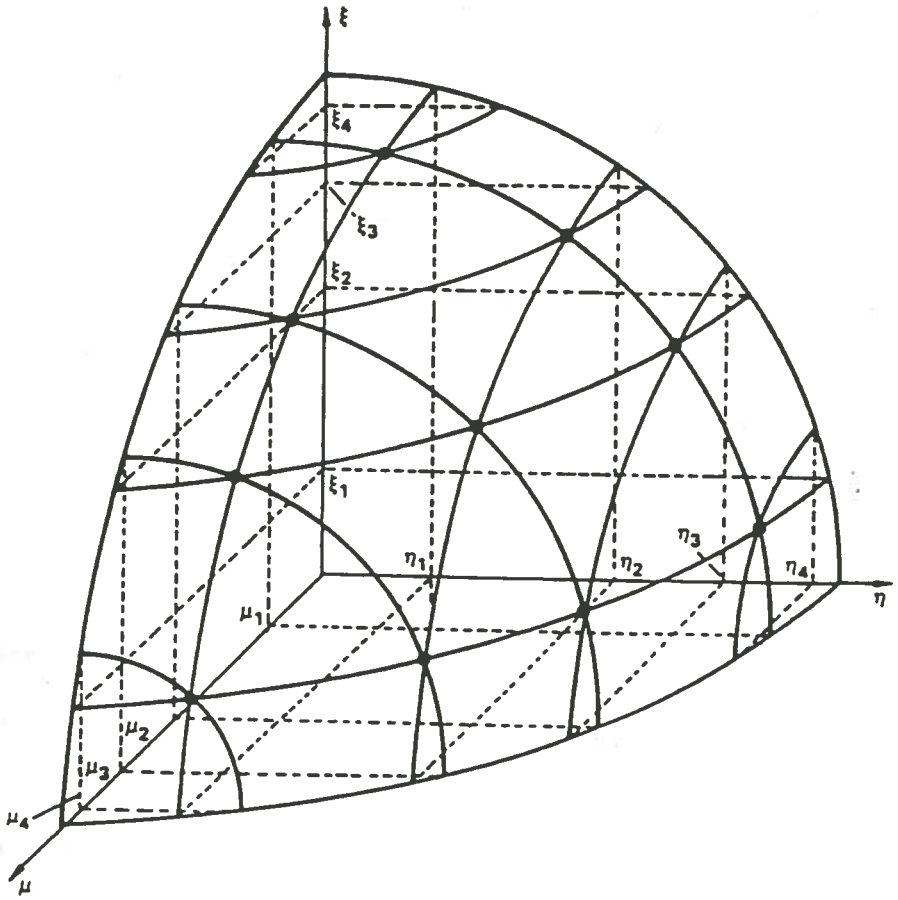

Fig. 3. A level symmetric S_8 discrete ordinates quadrature set

cosines with respect to each of the three axes; as a result, $\mu_1 = \eta_1 = \xi_1$, $\mu_2 = \eta_2 = \xi_2$, $\mu_3 = \eta_3 = \xi_3$, and $\mu_4 = \eta_4 = \xi_4$, etc. No axis, in this case, has any preference compared to the others, because the ordinate directions do not change with 90° rotations about any axis. The coordinates that have a direction cosine μ_n relative to the axis x_1 are located on the nth level relative to that axis; the same procedure applies for η_n and ξ_n. There are N(N+2)/8 ordinates in each octant and N(N+2) on the whole unit sphere[6].

The discrete ordinates angular flux for a direction $\hat{\Omega}_m$ is equal to 4π times the number of neutrons per cm^2 which pass through the area ΔA_m associated with $\hat{\Omega}_m$ per second. The scalar flux from its definition is given by[1]:

$$\Phi = \int_{4\pi} \Psi d\hat{\Omega} = \sum_{m=1}^{N} \Psi(\hat{\Omega}_m)\Delta\hat{\Omega}_m = \sum_{m=1}^{N}\Psi(\hat{\Omega}_m)W_m \quad - - - - - - - - - - - - - - - - \quad (9)$$

Defining the direction vector $\hat{\Omega}$ in curvilinear geometries (e.g., R-θ-Z) is somewhat different from that in cartesian geometries. In the curvilinear geometries $\hat{\Omega}$ is described in a local system of coordinates that depends on the spatial position. Since the direction variables continuously change for a streaming neutron in curvilinear geometry, extra terms containing derivatives with respect to the angular variable appear in the leakage term $\hat{\Omega}\cdot\nabla$ [see Eq. (4)]. The three components μ, η, ξ of the direction vector $\hat{\Omega}$ on R-θ-Z coordinates, respectively, are shown in fig. 1.

When a neutron experiences a scattering interaction, its direction of travel is altered. Consideration of anisotropic (i.e., non-symmetrical) scattering is very important in deep penetration problems

since forward directed scattering increases the penetrating capability. On the right-hand side of equation (3), the term $\Sigma_{sg'\rightarrow g}(\hat{\Omega}'\rightarrow\hat{\Omega})$ is the angle-dependent differential scatter cross section which relates the scatter of neutrons from an energy group g' traveling in direction $\hat{\Omega}'$ to an energy group g, traveling in direction $\hat{\Omega}$.

In the discrete ordinates method, anisotropic scattering is approximated by using a "Legendre cross section expansion". The angle-dependent differential scatter cross section is expanded in Legendre polynomials of the scatter cosine

$$\mu_o = \text{Cos}\theta = \hat{\Omega}'\cdot\hat{\Omega} \quad - - - - - - - - - - - - - - - - - - \quad (10)$$

where, $\hat{\Omega}'$ and $\hat{\Omega}$ are the initial and final directions, respectively, and θ is the scattering angle (fig. 4).

Usually, a 3rd order Legendre expansion gives a good approximation in most RPV transport theory calculations; thus, the differential scatter cross section is expressed as follows

$$\Sigma_{sg'\rightarrow g}(\mu_o) = \Sigma_{og'\rightarrow g}P_o + \Sigma_{1g'\rightarrow g}P_1(\mu_o) + \Sigma_{2g'\rightarrow g}P_2(\mu_o) + \Sigma_{3g'\rightarrow g}P_3(\mu_o) \quad - - - - - - - - - - - - \quad (11)$$

where the Legendre polynomials are given by

$$P_o = 1$$

$$P_1 = \mu$$

$$P_2 = \tfrac{1}{2}(3\mu^2-1)$$

$$P_3 = \tfrac{1}{2}(5\mu^3-3\mu)$$

The coefficients of the Legendre polynomials are called the "cross section moments." The 0th moment - $\Sigma_{og'\rightarrow g}$ - corresponds to the

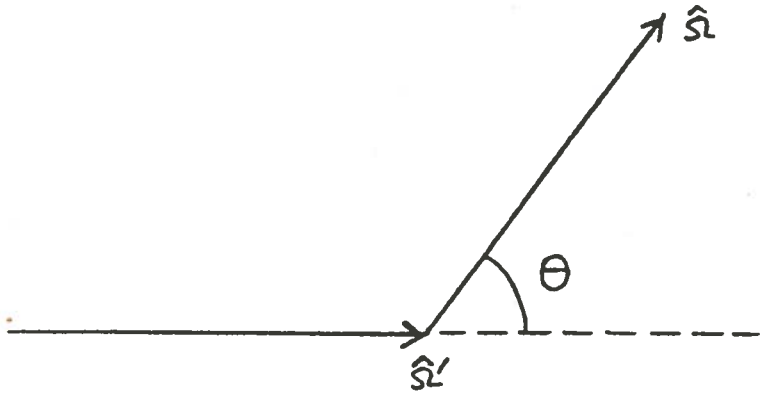

Fig. 4. Direction of neutron before and after scatter. $\hat{\Omega}'$ is the initial and $\hat{\Omega}$ is the final directions; θ is the scattering angle

group-to-group scatter cross-section matrix. The next moment, $\Sigma_{1g' \to g}$, is equal to three times the average cosine of scatter for a neutron going from energy g´ to g. The P_o cross section has all positive values; however, the other moments can be negative. The sum of all moments multipled by the corresponding Legendre polynomials should be positive for all values of μ_o, because this expression approximates the angle-dependent scatter cross section which is positive. In reality, negative values are sometimes obtained due to the finite number of terms in the expansion; but this shortcoming does not appear to affect the RPV flux calculation significantly.

2. Energy Discretization

To obtain an approximation to the transport equation in terms of the group angular flux, we first divide the continuous energy range of interest into G energy intervals (fig. 5). The particles in group "g" are those with energies between E_g and E_{g-1}; now we divide the energy integrals into the contribution for each energy group, i.e.,

$$\int_0^\infty dE = \sum_{g=1}^{G} \int_g dE \quad - \quad (12)$$

The multigroup angular flux is equal to

$$\Psi_g(\mathbf{r},\hat{\Omega}) = \int_g \Psi(\mathbf{r},\hat{\Omega},E)dE \quad - - - - - - - - - - - - - - - - - - \quad (13)$$

where,

$$\int_g dE = \int_{E_g}^{E_{g-1}} dE \quad - \quad (14)$$

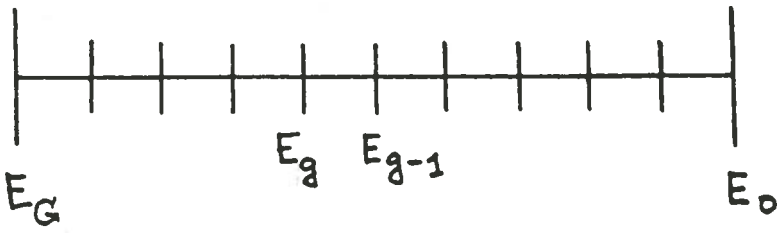

Fig. 5. Division of the whole energy range into several energy intervals

The multigroup form of the cross sections (σ_g, $\nu\sigma_{fg}$, $\sigma_{g'\to g}$) can be defined as follows

$$\sigma_g(\hat{r}) = \int_g \sigma(\hat{r},E) f_g(E)\,dE \quad \text{- - - - - - - - - - - - - - - - - - (15)}$$

where, $f_g(E)$ is the energy-dependent spectral weighting function which is normalized to unity:

$$\int_g f_g(E)\,dE = 1 \quad \text{- (16)}$$

To evaluate $f_g(E)$, we use some suitable approximation, such as

$$f_g(E) = \frac{w_g(E)}{\int_g w_g(E)\,dE} \quad \text{- (17)}$$

where, for example

$$w_g(E) = \chi(E) \equiv \text{fission spectrum, for } E > 100 \text{ KeV} \quad \text{- - - (18)}$$

$$= 1/E\Sigma_T(E) \equiv \text{narrow resonance approximation,}$$

$$1 \text{ eV} < E < 100 \text{ KeV} \quad \text{- - - - - - - - - - (19)}$$

$$= M(E) \equiv \text{Maxwellian, } E < 1 \text{ eV} \quad \text{- - - - - - - - - - - (20)}$$

Multigroup cross section libraries have been developed by various organizations, and are routinely available for transport calculations. For RPV flux analysis, 40 to 60 energy groups are typically employed.

3. Spatial Discretization

To spatially discretize, the domain is decomposed into a number of homogeneous cells. Now, instead of spatially continuous values of angular fluxes, a finite number of values describes the angular fluxes for a given neutron direction. These values correspond to the cell-averaged values over the mesh cell. All cross sections are assumed constant within each cell, but they may be different for different cells. Figures 6a and 6b show the basic mesh cells for R-θ-Z, R-θ, and R-Z geometries.

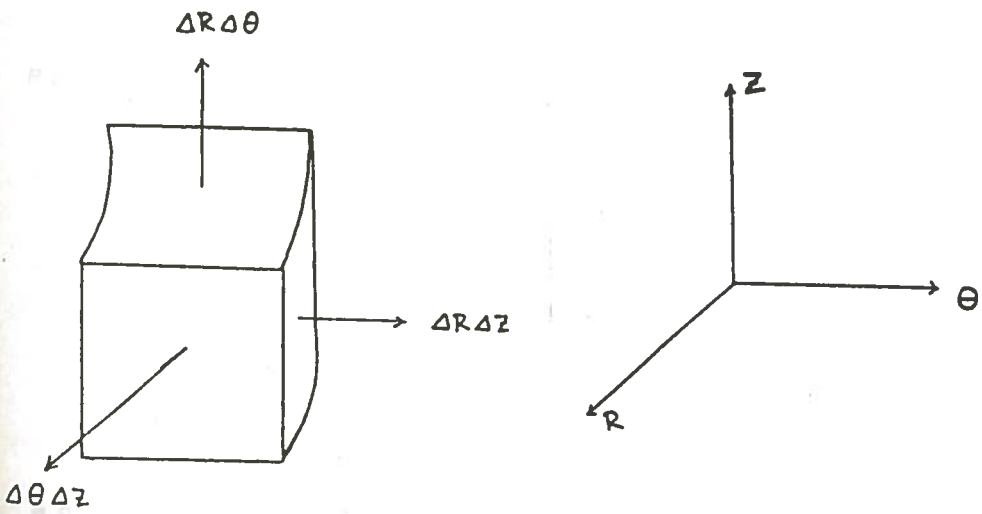

volume = $\Delta R \Delta\theta \Delta z$

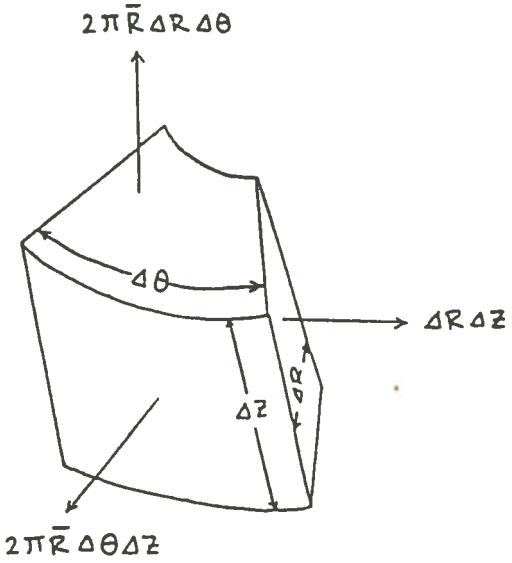

Fig. 6a. R-θ-Z volume elements (3-D mesh cells)

- RZ

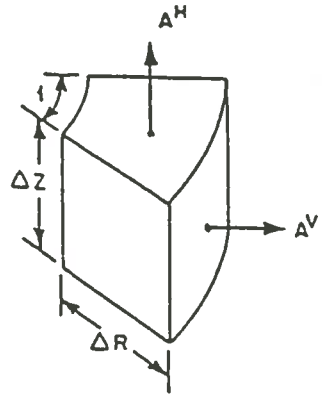

$A^V =$ $2\pi R(\Delta Z)$

$A^H =$ $2\pi \bar{R} \Delta R$

$V =$ $2\pi \bar{R} \Delta R(\Delta Z)$

- R θ

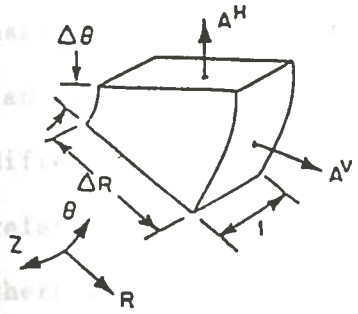

$2\pi R(\Delta\theta)$ ΔR $2\pi \bar{R} \Delta R(\Delta\theta)$

Fig. 6b. Two-dimensional mesh cells for R-Z and R-θ geometries

C. Three-Dimensional Flux Synthesis

As previously discussed, "synthesis" is an approximate method of obtaining a solution to some physical problem based on combining functions of a subset from the set of the independent variables associated with the problem[7].

Various approaches have been considered to approximate the multidimensional flux in reactor analysis. In some cases, a single 2-D expansion function for each axial zone is used. A more sophisticated method uses a linear combination of several 2-D expansion functions. Synthesis can be "single-channel" or "multi-channel." In multi-channel synthesis, different trial functions are used in different planar regions (usually referred to as "channels") as opposed to single-channel synthesis, where there is only one channel[7].

In this work, a single-channel synthesis method has been developed in which "channel fluxes" for R, R-Z and R-θ channels are used to obtain synthesized 3-D R-θ-Z scalar fluxes. The multigroup channel fluxes are defined as follows[8]

$$\Phi_{g,R} \equiv \Phi_g(R) = \int_{-\infty}^{+\infty} \int_{0}^{2\Pi} \Phi_g(R,\theta,Z)\,d\theta\,dZ \quad \text{- - - - - - - - - - - - - - - - (21)}$$

$$\Phi_{g,RZ} \equiv \Phi_g(R,Z) = \int_{0}^{2\Pi} \Phi_g(R,\theta,Z)\,d\theta \quad \text{- - - - - - - - - - - - - - - - - - (22)}$$

$$\Phi_{g,R\theta} \equiv \Phi_g(R,\theta) = \int_{-\infty}^{+\infty} \Phi_g(R,\theta,Z)\,dZ \quad \text{- - - - - - - - - - - - - - - - - (23)}$$

where, g - energy group index;

$\Phi_g(R)$ - radial (R) channel fluxes;

$\Phi_{g(R,Z)}$ - radial-axial (R-Z) channel fluxes;

$\Phi_{g(R,\theta)}$ - radial-azimuthal (R-θ) channel fluxes.

The function $\Phi_g(R,\theta,Z)$ in equations (21), (22), and (23) is assumed to be the true 3-D scalar flux distribution.

The scalar channel fluxes are related to the angular channel fluxes in the usual manner; for example,

$$\Phi_g(R,\theta) = \int_{4\Pi} \Psi_g(R,\theta,\hat{\Omega})d\hat{\Omega} \quad - \quad (24)$$

where,

$$\Psi_{g,R\theta} = \Psi_g(R,\theta,\hat{\Omega}) = \int_{-\infty}^{+\infty} \Psi_g(R,\theta,Z,\hat{\Omega})dZ \quad - - - - - - - - - - - - \quad (25)$$

It is important to note that for each energy group the three channel fluxes are related to each other in the following way:

$$\int_0^{2\Pi} \Phi_{g,R\theta}\, d\theta = \int_{-\infty}^{+\infty} \Phi_{g,RZ}\, dZ = \Phi_{g,R} \quad - - - - - - - - - - - - - - - - \quad (26)$$

1. Calculation of the Channel Fluxes

To obtain equations obeyed by the R-Z and R-θ channel angular fluxes, we integrate the 3-D (R-θ-Z) transport equation [equation (4)] over θ from 0 to 2Π and over Z from $-\infty$ to $+\infty$, respectively. For example, let us find the expression for the R-θ channel angular fluxes. When we integrate $\frac{\partial \Psi_g}{\partial Z}$ [see equation (4)] over Z from $-\infty$ to $+\infty$, we get zero, since the flux must vanish at $\pm\infty$. Thus, we have after integration,

$$\frac{\mu}{R}\frac{\partial(R\Psi_{g,R\theta})}{\partial R} + \frac{\eta}{R}\frac{\partial\Psi_{g,R\theta}}{\partial\theta} - \frac{1}{R}\frac{\partial(\eta\Psi_{g,R\theta})}{\partial\omega} +$$

$$\int_{-\infty}^{+\infty} \Sigma_{Tg}\,\Psi_g(R,\theta,Z,\hat{\Omega})dZ =$$

$$\sum_{g'}\int_{\hat{\Omega}'}\int_{-\infty}^{+\infty}\Sigma_{sg'\to g}(\hat{\Omega}'\to\hat{\Omega})\Psi_{g'}(R,\theta,Z,\hat{\Omega}')d\hat{\Omega}'dZ + \int_{-\infty}^{+\infty}Q_g dZ \quad \text{- - - - - - - - -} \quad (27)$$

We now define the axially averaged total and group-to-group scatter cross sections as follows:

$$\bar{\Sigma}_{Tg}(R,\theta,\hat{\Omega}) = \frac{\int_{-\infty}^{+\infty}\Sigma_{Tg}\Psi_g(R,\theta,Z,\hat{\Omega})dZ}{\int_{-\infty}^{+\infty}\Psi_g(R,\theta,Z,\hat{\Omega})dZ} \quad \text{- - - - - - - - - - - - - - - -} \quad (28)$$

and

$$\bar{\Sigma}_{sg'\to g}(R,\theta,\hat{\Omega}'\to\hat{\Omega}) = \frac{\int_{-\infty}^{+\infty}\Sigma_{sg'\to g}(\hat{\Omega}'\to\hat{\Omega})\Psi_{g'}(R,\theta,Z,\hat{\Omega}')dZ}{\int_{-\infty}^{+\infty}\Psi_{g'}(R,\theta,Z,\hat{\Omega}')dZ} \quad \text{- - - - - - -} \quad (29)$$

As we can see, the angular fluxes that appear in equations (28) and (29) introduce a direction dependence ($\hat{\Omega}$) to the average cross sections (as with all multigroup transport developments). This is undesirable and can be overcome by using an approximate flux distribution; e.g., the angular fluxes are replaced by the scalar fluxes, thus obtaining the following:

$$\bar{\Sigma}_{Tg}(R,\theta) = \frac{\int_{-\infty}^{+\infty}\Sigma_{Tg}\Phi_g(R,\theta,Z)dZ}{\int_{-\infty}^{+\infty}\Phi_g(R,\theta,Z)dZ} \quad \text{- - - - - - - - - - - - - - - - - -} \quad (28a)$$

and

$$\bar{\Sigma}_{sg'\to g}(R,\theta,\hat{\Omega}'\to\hat{\Omega}) = \frac{\int_{-\infty}^{+\infty} \Sigma_{sg'\to g}(\hat{\Omega}'\to\hat{\Omega})\phi_{g'}(R,\theta,Z)dZ}{\int_{-\infty}^{+\infty} \phi_{g'}(R,\theta,Z)dZ} \quad - - - - - - \quad (29a)$$

This approximation amounts to assuming that the angular and the scalar fluxes have the same axial variations at a given R,θ point.

Equation (27) now becomes

$$\frac{\mu}{R}\frac{\partial(R\Psi_{g,R\theta})}{\partial R} + \frac{\eta}{R}\frac{\partial\Psi_{g,R\theta}}{\partial\theta} - \frac{1}{R}\frac{\partial(\eta\Psi_{g,R\theta})}{\partial\omega} + \bar{\Sigma}_{Tg}(R,\theta)\phi_{g,R\theta}$$

$$= \sum_{g'}\int_{\hat{\Omega}'} \bar{\Sigma}_{g'\to g}(\hat{\Omega}'\to\hat{\Omega})\phi_{g',R\theta}\, d\hat{\Omega}' + Q'_g \quad - - - - - - - - - - - - - - \quad (30)$$

where,

$$Q'_g = \int_{-\infty}^{+\infty} Q_g dZ \quad - \quad (31)$$

(the source is zero outside the core region).

The same procedure applies to obtaining an equation for the R-Z channel fluxes. If the "exact" channel average cross sections are used, then equation (30) gives the exact R-θ channel fluxes.

In reality, the exact channel average cross sections are not known, since these are weighted by the unknown scalar flux distribution. If the macroscopic cross sections do not vary strongly in θ or Z, which is usually the case for RPV fluence calculations, then the channel average cross sections appearing in the R-θ channel equation are not very sensitive to the axial weight function; so that crude approximations for the scalar flux variation are adequate to obtain the weighted cross sections. In fact, in the usual case for the ex-core region, where the total and

the group-to-group scatter cross sections are almost invariant axially (over the height of interest), axial weighting of these cross sections is not needed. This situation is characteristic to most PWRs in the high-energy range, assuming that the concentration of water and structural materials are approximately uniform axially. The non-fuel nuclides have the largest macroscopic cross sections in this energy range. On the other hand, if cross sections do vary axially, then axial weighting can actually be performed, if desired, by using an approximate axial flux distribution. For example, the known neutron source distribution along the axial direction can be used as a weight function. A simpler way is to merely smear the cross sections over the axial direction. This assumes a flat axial flux distribution. In fact, previous reactor studies have shown that, in most practical cases, the axial weighting has almost no effect on the ultimate results[8].

Equation (30) is identical to the standard R-θ transport equation solved by the 2-D discrete ordinates transport code DOT-IV[8]. Therefore in practice, R-θ channel fluxes can be obtained from a DOT-IV R-θ calculation. The midplane values of the macroscopic cross sections or one of the other weighting approximations discussed previously can be taken as the axially averaged cross sections, and the R-θ channel source is obtained by simply integrating the known 3-D (R-θ-Z) source over Z - the axial direction. In a similar way, the R-Z channel fluxes are calculated by DOT-IV where the R-Z source is obtained by merely integrating the known 3-D (R-θ-Z) source over the azimuthal direction; and cross sections are weighted, in a similar fashion, over the azimuthal direction.

In a similar manner, by solving the 1-D radial transport equation we can find 1-D channel fluxes. In determining the 1-D channel transport

equation, the R-Θ-Z transport equation is integrated over both Z and Θ directions, the source being integrated over Z and Θ directions and the cross sections weighted over both Z and Θ directions. The 1-D source can equivalently be found by integrating the R-Z channel source over the axial direction. Note from equation (26) that the R channel fluxes could also be obtained by integrating the DOT-IV R-Z fluxes over the axial direction, e.g.,

$$\Phi_R = \int_{Z_L}^{Z_U} \Phi_{RZ} dZ \quad \text{-----------------------} \quad (32)$$

where Z_L and Z_U are the lower and upper limits of integration. In this case, the axial limits Z_L and Z_U should be large enough so that

$$\int_{Z_L}^{Z_U} \Phi_{RZ} dZ \cong \int_{-\infty}^{+\infty} \Phi_{RZ} dZ \quad \text{----------------------} \quad (33)$$

This approximation follows directly from Equation (26). Unfortunately, this approximation usually underestimates the radial channel fluxes, because the R-Z channel flux falls off slowly in the Z direction, consequently preventing expression (33) from being very accurate unless Z_U and Z_L are very large. Often the upper and lower Z values used in R-Z channel flux calculation do not satisfy this condition.

2. Synthesis Approximation in R-Θ-Z System of Coordinates

We now define the synthesized 3-D flux as a function of R,Θ,Z variables for the cylindrical geometry to be[8]

$$\Phi_{sg}(R,\Theta,Z) \simeq \frac{\Phi_g(R,Z)*\Phi_g(R,\Theta)}{\Phi_g(R)} \quad \text{-----------------} \quad (34)$$

where, $\Phi_{sg}(R,\Theta,Z) \equiv$ multigroup synthesized 3-D flux.

This synthesis approximation is simple, and by only one multiplication and one division, the desired synthesized flux can be found if the channel fluxes are provided.

Although equation (34) is an approximate expression, it becomes exact if the flux is separable either azimuthally or axially. For example, if the flux is separable azimuthally, we have

$$\Phi_g(R,\theta,Z) = A_g(R,Z)*B_g(\theta) \quad - \quad (35)$$

Then from equations (21), (22), (23), and (34), we can write

$$\Phi_{sg}(R,\theta,Z) = \frac{\int_0^{2\pi} A_g(R,Z)*B(\theta)d\theta * \int_{-\infty}^{+\infty} A_g(R,Z)*B_g(\theta)dZ}{\int_{-\infty}^{+\infty} A_g(R,Z)dZ * \int_0^{2\pi} B_g(\theta)d\theta}$$

$$= \frac{A_g(R,Z)\int_0^{2\pi} B_g(\theta)d\theta * B_g(\theta)\int_{-\infty}^{+\infty} A_g(R,Z)dZ}{\int_{-\infty}^{+\infty} A_g(R,Z)dZ * \int_0^{2\pi} B_g(\theta)d\theta}$$

$$= A_g(R,Z)*B_g(\theta) = \Phi_g(R,\theta,Z) \quad - - - - - - - - - - - - - - \quad (36)$$

In the same manner, it can be shown, that equation (34) is exact if the flux is separable axially.

In the case where the flux is not separable, equation (34) always preserves the integrated values of the flux in both the axial and azimuthal directions at all radial points. This is shown below.

Let us integrate equation (34) over Z at some arbitrary location R. We get

$$\int_{-\infty}^{+\infty} \Phi_{sg}(R,\theta,Z)dZ = \frac{\int_{-\infty}^{+\infty} \Phi_g(R,Z)dZ * \phi_g(R,\theta)}{\Phi_g(R)} \quad \text{- - - - - - - - - - - - - (37)}$$

From equation (26),

$$\int_{-\infty}^{+\infty} \Phi_g(R,Z)dZ = \Phi_g(R)$$

Therefore, equation (37) can be written in the following way:

$$\int_{-\infty}^{+\infty} \Phi_{sg}(R,\theta,Z)dZ = \frac{\Phi_g(R) * \phi_g(R,\theta)}{\Phi_g(R)}$$

$$= \Phi_g(R,\theta) = \int_{-\infty}^{+\infty} \Phi_g(R,\theta,Z)\, dZ \quad \text{- - - - - - - - - - (38)}$$

Equation (38) is exactly the same as equation (23), thus proving that the synthesized 3-D flux has the same integrated value as the true 3-D flux at all radial points.

Equation (34) is essentially a single-channel synthesis approximation for $\Phi_g(R,\theta,Z)$. The term corresponding to

$$A_g(R,Z) = \frac{\Phi_g(R,Z)}{\Phi_g(R)} \quad \text{- (39)}$$

can be viewed as the axial distribution factor at each R point, which distributes the axially-integrated flux ($\Phi_{R\theta}$) over the Z dimension.

D. Three-Dimensional Synthesis Code - DOTSYN

The computer code DOTSYN[8], developed as part of this study, functions as a module in the LEPRICON computer code system which is distributed by the Electric Power Research Institute (EPRI) to U.S. utilities for RPV fluence analysis. The flow chart of the LEPRICON computer code system is shown in fig. 7. DOTSYN, as a vital part of this system, accomplishes the 3-D flux synthesis and activity calculations for various dosimeter materials used in the RPV surveillance program. The synthesis methodology corresponds to that discussed in the previous section. The code is designed to be coupled with DOT-IV output for the channel fluxes, and can treat "variable mesh" problems from DOT.

1. Programming Methodology

DOTSYN is written in FORTRAN programming language. Variably dimensioned arrays have been used to minimize storage requirements. The convenient free-form input system FIDO is used for entering data[1]. The flow chart in fig. 8 shows the sequence of calculations in DOTSYN.

As seen from the flow chart, there are two calculational parts in the program. The first part consists of calculation of the synthesized 3-D fluxes for the number of energy groups desired. A synthesis region is specified by user input. In performing the synthesis for each energy group, the channel fluxes for R-θ, R-Z, and 1-D (R) are read from the respective logical units or cards as required [see input description in Appendix E], and the synthesis calculation is done according to equation (34) for each discrete point. This is done in the following manner:

In the synthesis region, for a given azimuthal interval at a given axial level, synthesis is performed for all the radial intervals

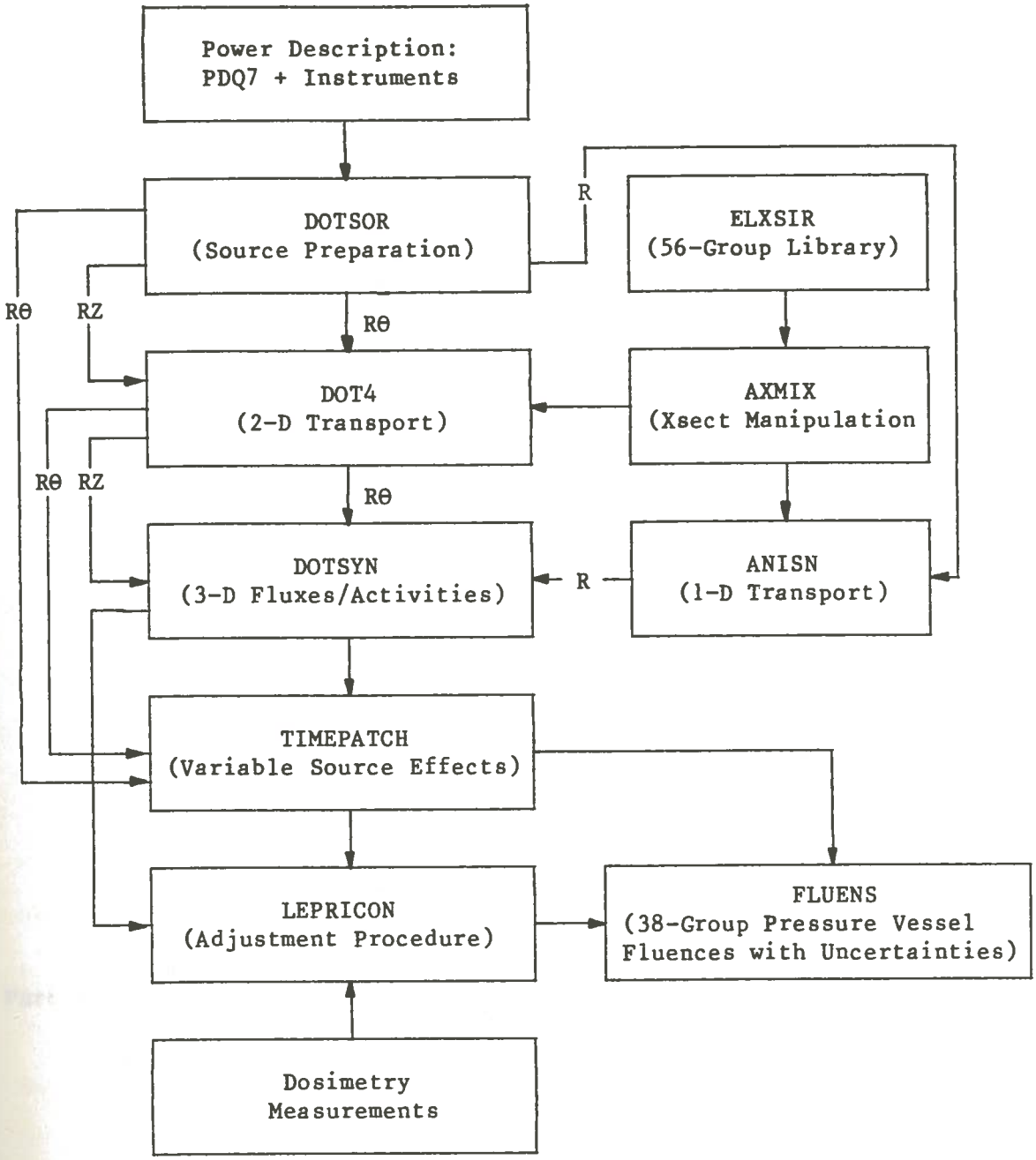

Fig. 7. LEPRICON System Flow Chart

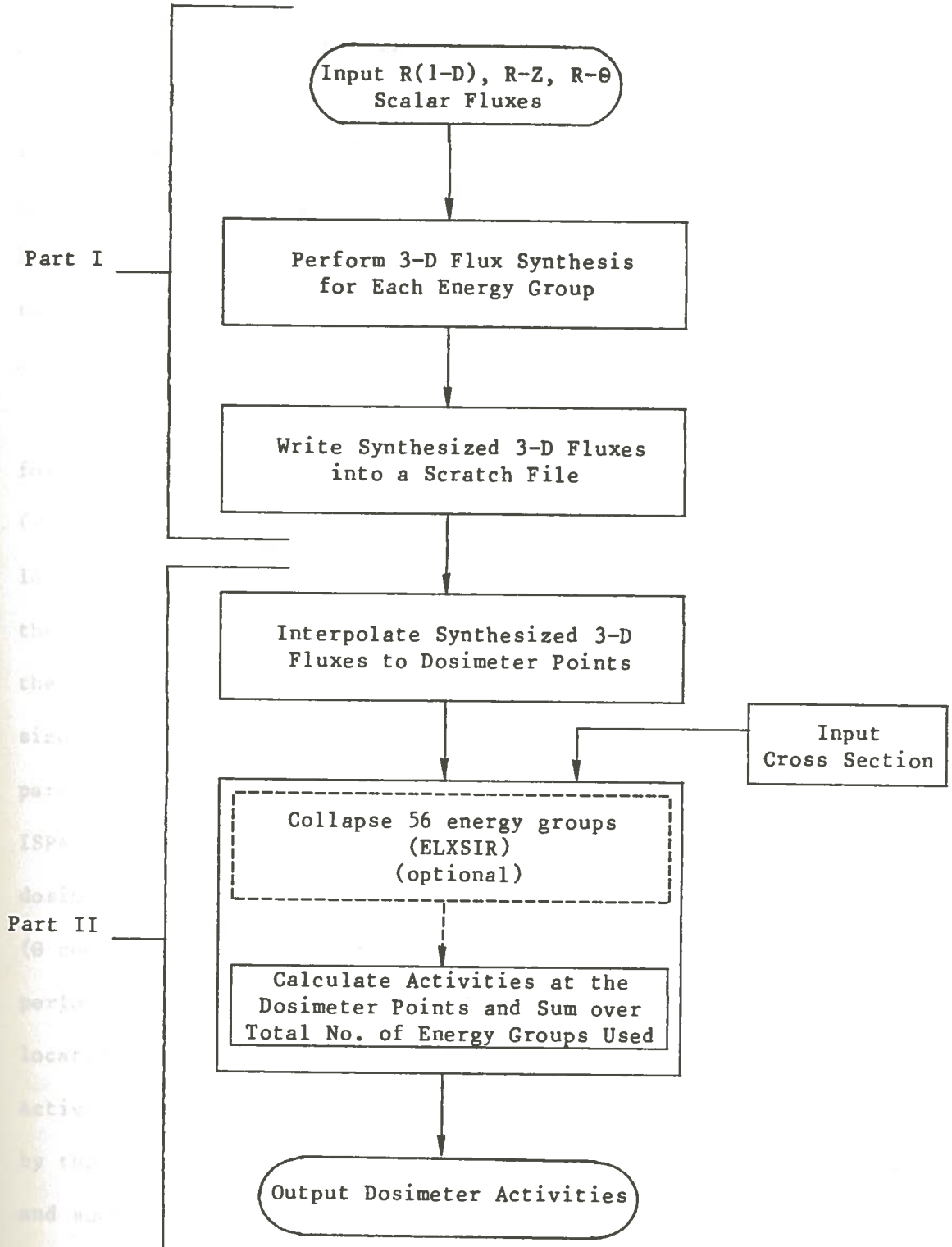

Fig. 8. Sequence of Calculations in DOTSYN

contained in that azimuthal interval. This procedure is repeated for all successive azimuthal intervals keeping the axial level fixed. The whole procedure, described above is now repeated for all subsequent axial levels. These steps are followed for all the energy groups. The fluxes calculated in this way are stored on a scratch file (logical unit 8) in binary form. Each record in this data set has the fluxes computed at all radial and azimuthal intervals, corresponding to a fixed axial level for a given energy group. This procedure saves core storage requirements.

In the second part of the routine, activities (e.g., reaction rates) for different dosimeter materials, for a given number of experiment (dosimeter) locations are computed using the synthesized fluxes calculated in the first part. Dosimeter locations must be contained within the synthesis region. There is an option in the program which allows the user to compute activities at all the locations for which synthesized 3-D fluxes have been calculated. This option in invoked when the parameter ISPAR(3) is equal to -1. In the input description, parameter ISPAR(2) specifies the number of dosimeter locations. For the ISPAR(2) dosimeter locations [specified in the arrays 16** (R coordinates), 17** (θ coordinates) and 18** (Z coordinates)] a linear interpolation is performed to get the synthesized 3-D flux at the specified dosimeter location, if this location does not coincide with an interval midpoint. Activities are calculated by multiplying the 3-D flux (at that location) by the respective activation cross section of the dosimeter material, and summing over energy groups.

Two important points need to be mentioned here:

(i) in the synthesis region, the R coordinates for R-Z geometry and R-θ geometry must coincide. In other words, variable R-θ meshes are

allowed, but the R coordinates in R-θ and R-Z geometries have to be the same in the synthesis region. The R coordinates in 1-D (R) geometry must also coincide with those in the R-Z geometry. This should be taken care of during the DOT-IV runs for the channel fluxes.

(ii) During the activity calculations, the Z coordinates for the dosimeter locations in the 18** array must be in increasing order.

2. Execution of DOTSYN

A simple main program assigns the total core storage needed for DOTSYN. This is defined by the container array D, which is dimensioned by the core storage required and specified by the user for each particular problem. DOTSYN calculates the storage required for input and calculations; if the total storage is less than that provided, DOTSYN terminates the execution with a message of "insufficient storage".

CHAPTER III

TRANSPORT CALCULATIONS IN R-Θ-Z SYSTEM OF COORDINATES

In order to validate the synthesis approximation, a typical PWR reactor has been modeled in R, Θ and Z dimensions. The reactor model is based on a similar configuration to the Babcock and Wilcox Arkansas Nuclear One Unit-1 (ANO-1) reactor. Because of azimuthal symmetry, only 1/8th of the reactor has been considered. The outer radius extends from the core center past the pressure vessel. The 3-D code TORT is used to analyze this configuration to provide a reference 3-D "benchmark" solution to which the synthesis results will be compared. The synthesis results require determining the 2-D R-Θ and R-Z channel fluxes with the 2-D transport code DOT-IV. In this section, the 3-D and 2-D models, needed for the discrete ordinates transport calculations, are developed.

A. Model Configurations of the Reactor

The cross-sectional view of the reactor vessel and internals of the ANO-1 nuclear reactor is shown in fig. 9, and fig. 10 shows the vertical cross section of this reactor.

The configuration consists of 177 fuel assemblies in the core, which is surrounded by a 1.91-cm-thick stainless steel baffle. A stainless steel core barrel of inner diameter 358.14 cm surrounds the baffle. Outside the core barrel is a stainless steel thermal shield. There are four surveillance specimen holder tubes attached to the outer side of the thermal shield. Water flows downward through the downcomer region

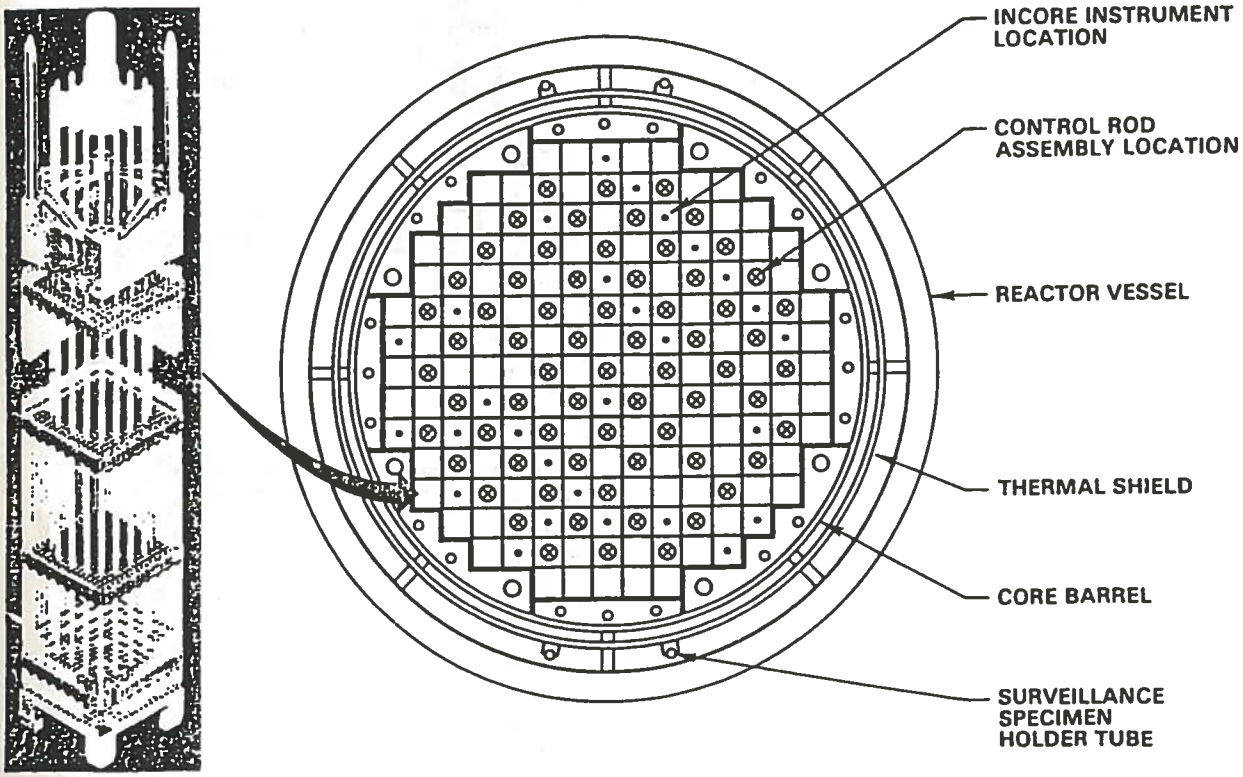

Fig. 9. Cross-sectional view of ANO-1 nuclear reactor

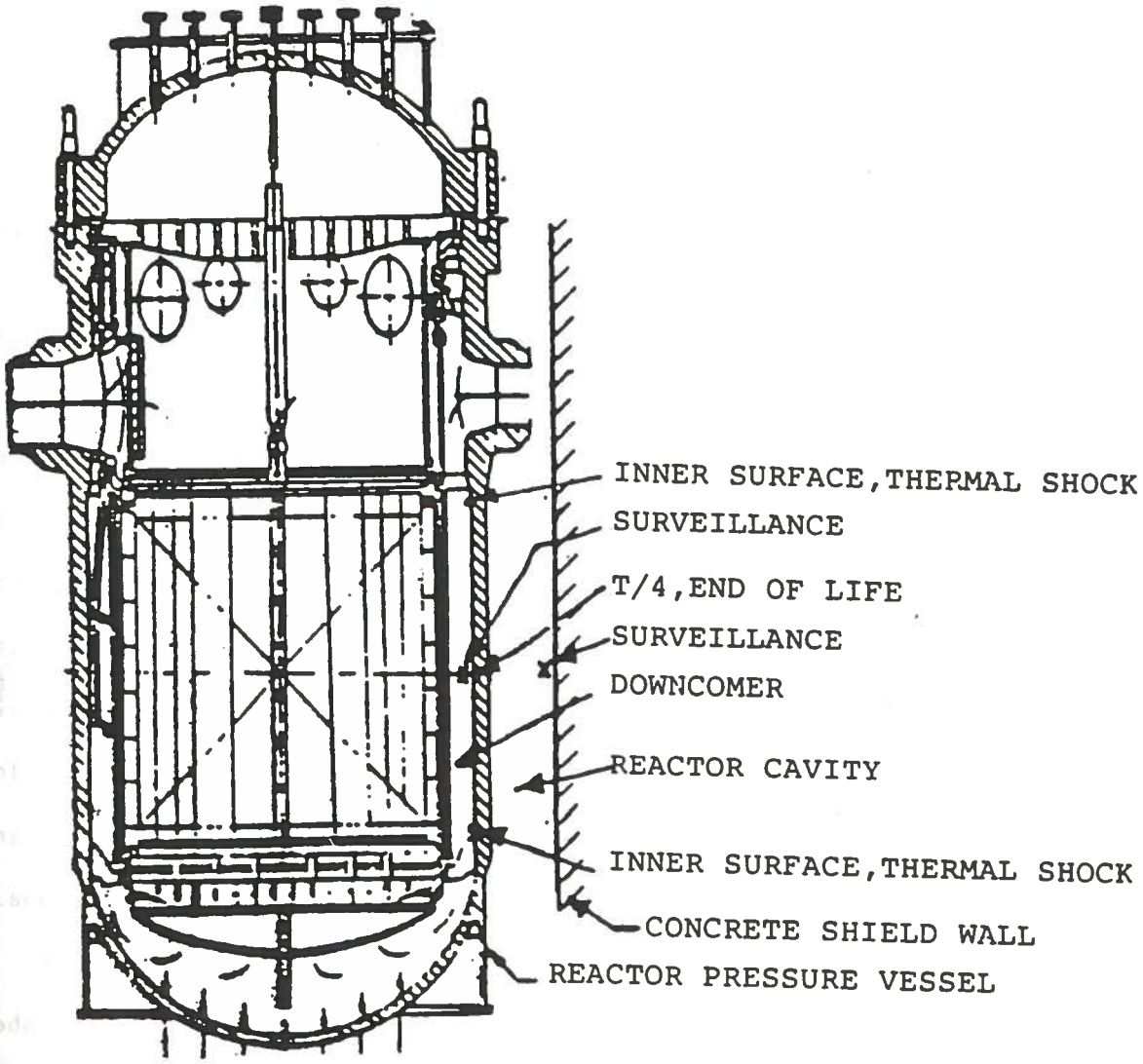

Fig. 10. Cut-away view of ANO-1 showing the pressure vessel and other components

between the thermal shield and the carbon steel reactor pressure vessel (RPV). Some of the core design, thermal and hydraulic data of ANO-1 are given in table 1. A somewhat simplified version of the actual reactor has been used as a calculational model in the present study. S_6 quadrature sets have been used in all calculations.

1. The R-θ-Z Model

A 1/8th segment of the ANO-1 nuclear reactor in three dimensions is shown in fig. 11. This 3-D model is used for the 3-D transport calculations by TORT. TORT is the 3-D version of the 2-D discrete ordinates transport code DOT-IV. The current version of TORT is still at the experimental stage, and has not been made available to the public. LSU was given special permission by ORNL to use the code in this study. Unfortunately, TORT does not currently have the option to use a reflecting upper θ (at 45°) boundary condition - a difficulty which will be discussed later in this chapter.

There are 55 radial, 33 azimuthal and 40 axial intervals in the model used to represent the reactor in three dimensions. A total of 11 different regions have been identified with eight different material compositions. A P_3 Legendre expansion of the cross section is employed. Input data to TORT for the 3-D transport calculations is given in Appendix D.

2. The R-θ Model

The R-θ model[9] of the reactor used in the DOT-IV transport calculations of the R-θ fluxes is shown in fig. 12 and fig. 13. There are 55 radial intervals and 33 azimuthal intervals for a 45° slice. A reflecting boundary condition is used along the 0° line. Usually a reflecting boundary condition is used along the 45° line as well; but in the newly

TABLE 1

Core design, Thermal, and Hydraulic Data for ANO-1

Reactor	
Design Heat Output, MWth	2599.6
Vessel Coolant Inlet Temperature, Deg. F	554
Vessel Coolant Outlet Temperature, Deg. F	603.8
Core Outlet Temperature, Deg. F	606.2
Core Operating Pressure, psig	2185
Core and Fuel Assemblies	
Total Number of Fuel Assemblies in Core	177
Number of Fuel Rods per Fuel Assembly	208
Number of Control Rod Guide Tubes per Assembly	16
Number of In-Core Instrument Positions per Fuel Assembly	1
Fuel Rod Outside Diameter, in.	0.430
Cladding Thickness, in.	0.0265
Fuel Rod Pitch, in.	0.568
Fuel Assembly Pitch Spacing, in.	8.587
Unit Cell Metal/Water Ratio (Volume Basis)	0.82
Cladding Material	Zircaloy-4 (Cold Worked)
Fuel	
Material	UO_2
Form	Dished-End, Cylindrical Pellets
Pellet Diameter, in.	0.370
Active Length, in.	144
Density, % of Theoretical	92.5

TABLE 1 (continued)

Heat Transfer and Fluid Flow at Design Power	
Total Heat Transfer Surface in Core, ft^2	49,734
Average Heat Flux, $Btu/h\text{-}ft^2$	171,470
Maximum Heat Flux, $Btu/h\text{-}ft^2$	534,440
Average Power Density in Core, KW/ℓ	83.39
Average Thermal Output, KW/ft of Fuel Rod	5.66
Maximum Thermal Output, KW/ft of Fuel Rod	17.63
Maximum Cladding Surface Temperature, Deg. F	654
Average Core Fuel Temperature, Deg. F	1280
Maximum Fuel Central Temperature at Hot Spot, Deg. F	4220
Total Reactor Coolant Flow, lb/h	131.32×10^6
Core Flow Area (Effective for Heat Transfer), ft^2	49.19
Core Coolant Average Velocity, fps	15.73
Coolant Outlet Temperature at Hot Channel, Deg. F	647.1
Power Distribution	
Maximum/Average Power Ratio, Radial x Local ($F\Delta h$ Nuclear)	1.78
Maximum/Average Power Ratio, Axial (F_z Nuclear)	1.70
Overall Power Ratio (F_q Nuclear)	3.03
Power Generated in Fuel and Cladding, %	97.3

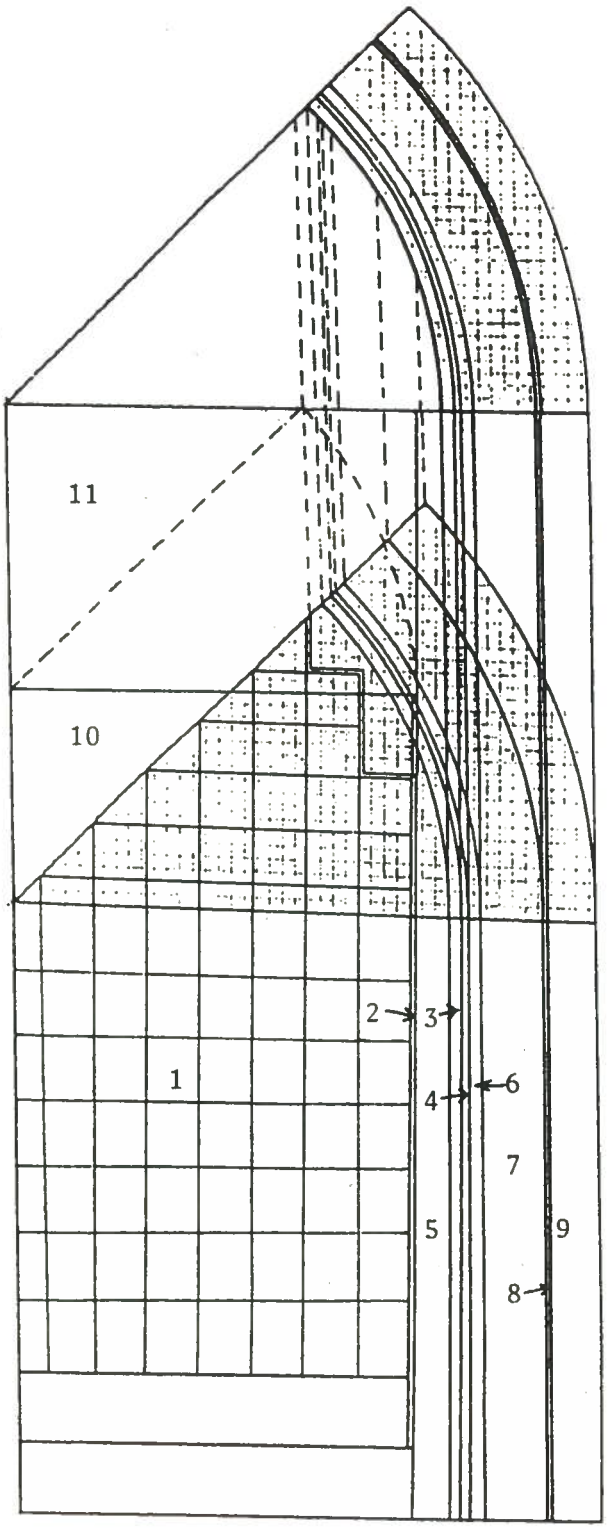

1 - core
2 - baffle
3 - barrel
4 - water gap
5 - radial reflector
6 - thermal shield
7 - downcomer
8 - RPV liner
9 - RPV
10 - upper reflector region
11 - upper reflector steel region

Fig. 11. 1/8th segment of ANO-1 nuclear reactor in three dimensions (R-θ-Z). Zones are shown by numbers

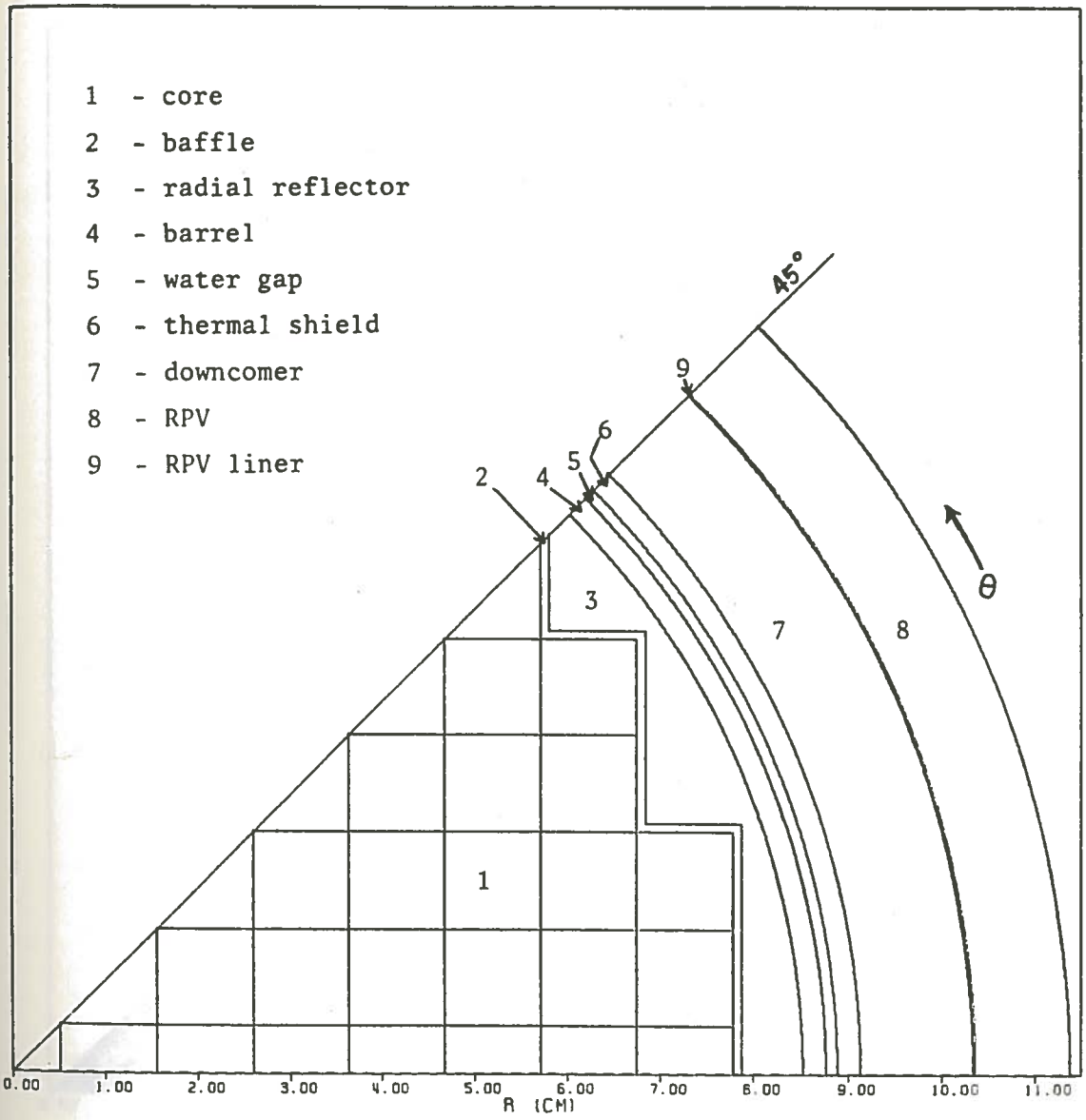

Fig. 12. 1/8th slice of ANO-1 nuclear reactor up to pressure vessel (top view). Zones are shown by numbers. scale: 1.0 cm = 21.0 cm

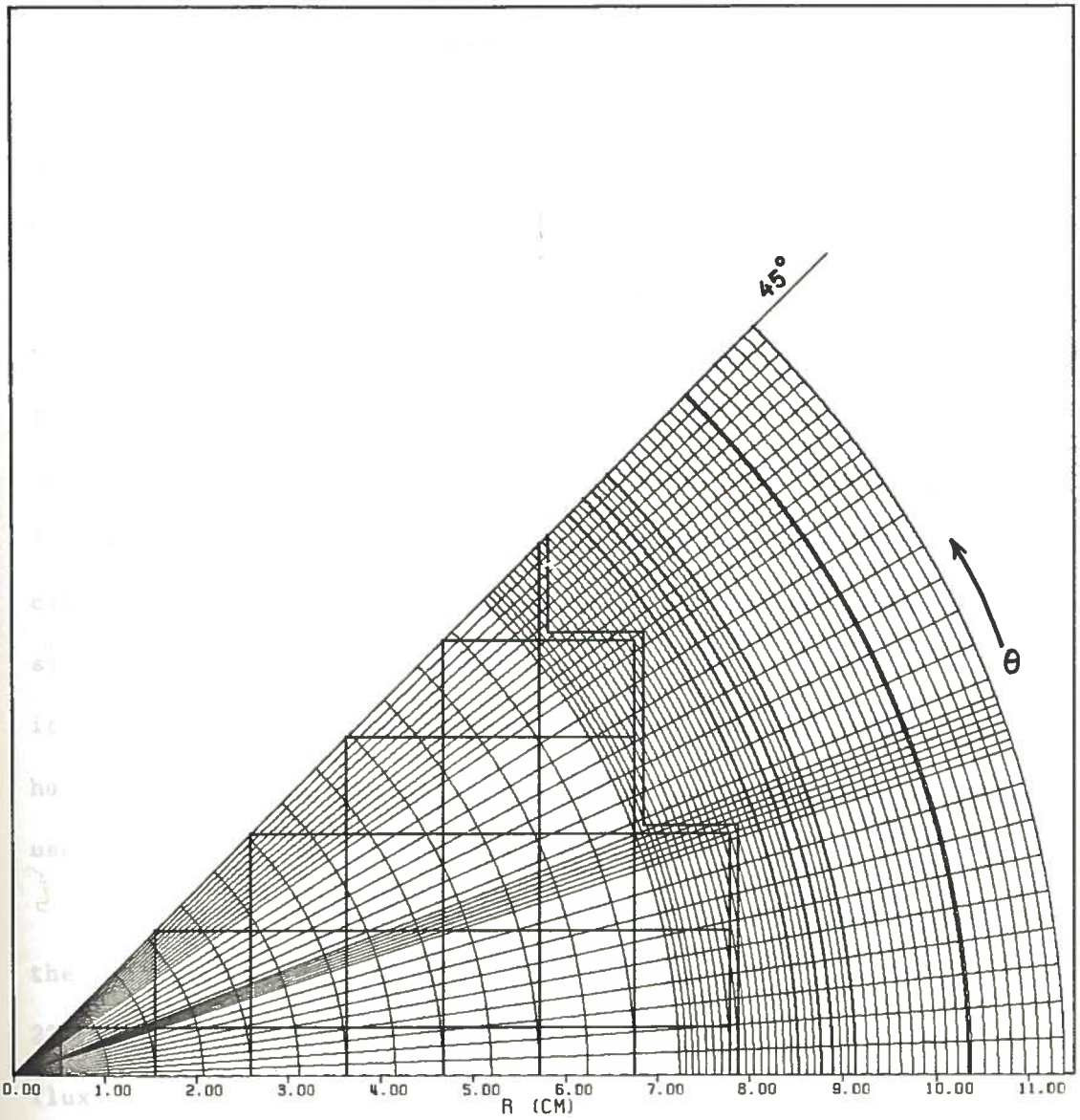

Fig. 13. R-θ representation of ANO-1 (1/8th slice up to pressure vessel) (top view)
scale: 1.0 cm = 21.0 cm

developed 3-D Oak Ridge Transport Code TORT, this boundary condition has not been incorporated yet, and consequently, only a vacuum boundary condition can be treated in the benchmark 3-D solution. Obviously, this boundary condition is not realistic for actual power reactors. However, the flux at azimuthal locations far from the 45° boundary (i.e., near 0°) is not sensitive to the outer boundary condition, and the calculated values should be valid in this region. Furthermore, the objective of this study is to validate the synthesis approximation, rather than to obtain actual, realistic flux values. Therefore, the important factor is consistency in the treatment of the boundary condition in the 3-D calculations and the 2-D calculations of the channel fluxes for the synthesis approximation, rather than the specific boundary condition itself. Therefore, in the DOT-IV R-θ model, a void boundary condition has been used along the 45° line to make the model consistent with that used in TORT.

It has been verified numerically that the results with the void and the reflected boundary conditions at 45° agree well from 0° up to about 22° in the R-θ model for radial points away from the origin. The azimuthal flux variation obtained with DOT-IV at the pressure vessel inner surface is shown in fig. 14 for each boundary condition. It can be seen that at 22°, the fluxes obtained with the two boundary conditions agree to 1.28%. All the pertinent input data to DOT-IV for the R-θ calculations are given in Appendix A.

Usually for a 45° slice, about 60 azimuthal and 100 radial intervals are used in order to represent the edge of the core as accurately as possible. But since the main purpose of this study is just to compare the approximate results produced by DOTSYN with those produced by TORT,

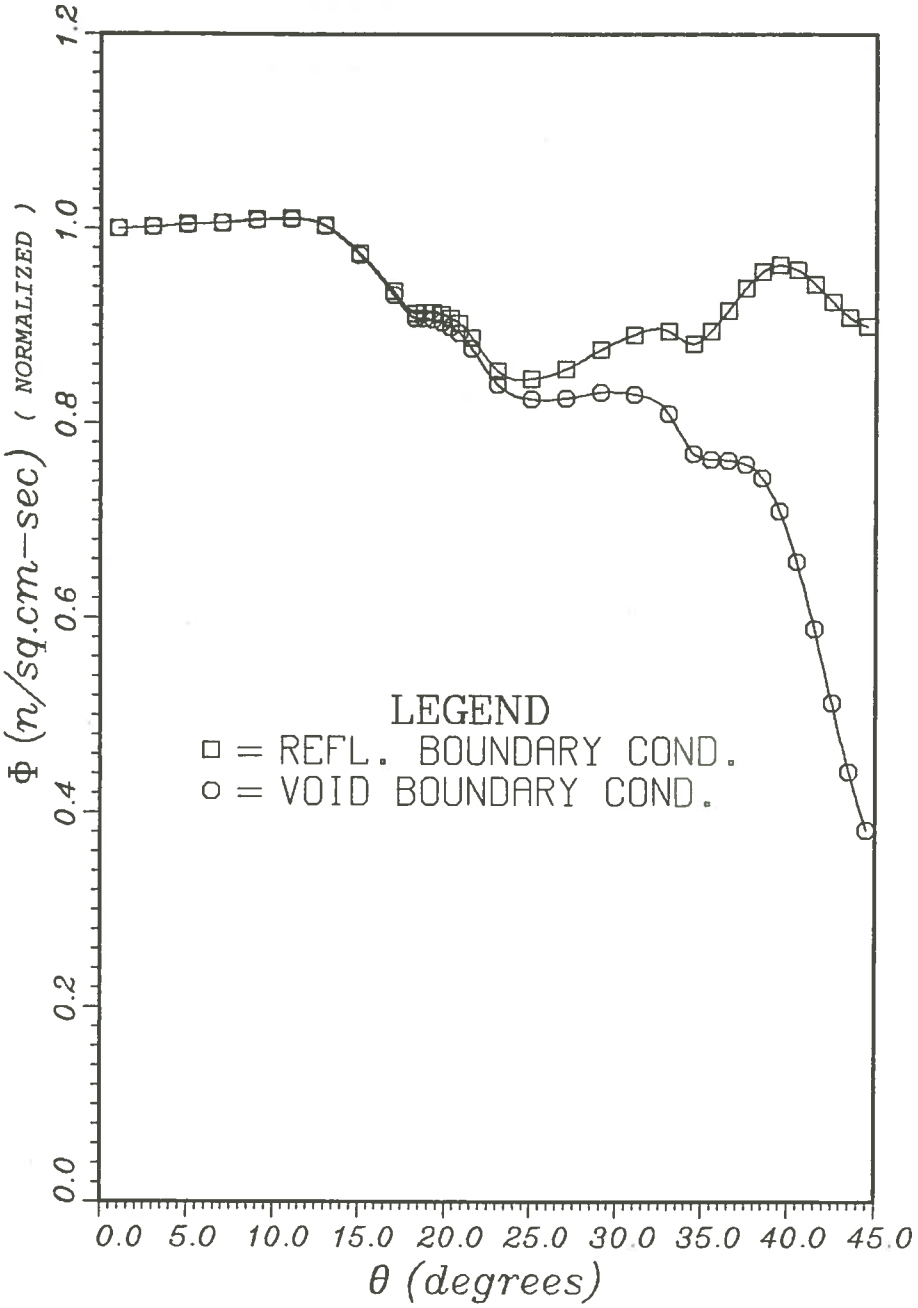

Fig. 14. R-θ fluxes at the pressure vessel inner surface with different boundary conditions at the top θ (45°)

only 55 radial and 33 azimuthal intervals are used in all calculations. This relatively coarse mesh approximates the core fairly accurately as can be seen in fig. 15. For simplicity and to save computer time, it was necessary to use a smaller number of intervals. There are 21 radial intervals in the core region and 8 in the RPV region. There are in total 9 regions in the R-θ model, shown in fig. 12. by numbers.

3. The R-Z Model

The R-Z model of the reactor used in the DOT-IV calculations of the R-Z channel fluxes is shown in fig. 16 and fig. 17. For this model, the transport calculations have been performed from the core midplane to the nozzle top, because the reactor is assumed symmetrical about the midplane. This reduces the number of axial intervals by half which consequently saves computer time. In reality, the core is not exactly symmetrical, but this approximation is quite adequate for the purpose of this study. The section from the core centerline up to the nozzle has been divided into 40 intervals (fig. 17) - 15 intervals in the core region (from the core centerline up to the core top), 10 intervals in the upper reflector region (region 2 in fig. 16) and 15 intervals in the upper reflector steel region (region 3 in fig. 16). The number of radial intervals has been taken to be the same as for the R-θ model, i.e., 55. All input data to DOT-IV for the R-Z calculation are given in Appendix B. There are 11 regions in the R-Z model as shown by the numbers in fig. 16. The R-Z model corresponds, in fact, to a full cylinder, unlike the R-θ model which corresponds to only 1/4th core (due to the void boundary condition at the 45° boundary); therefore, a different normalization factor will be associated with the R-Z and the R sources compared to the R-θ source. However, as long as they are consistent,

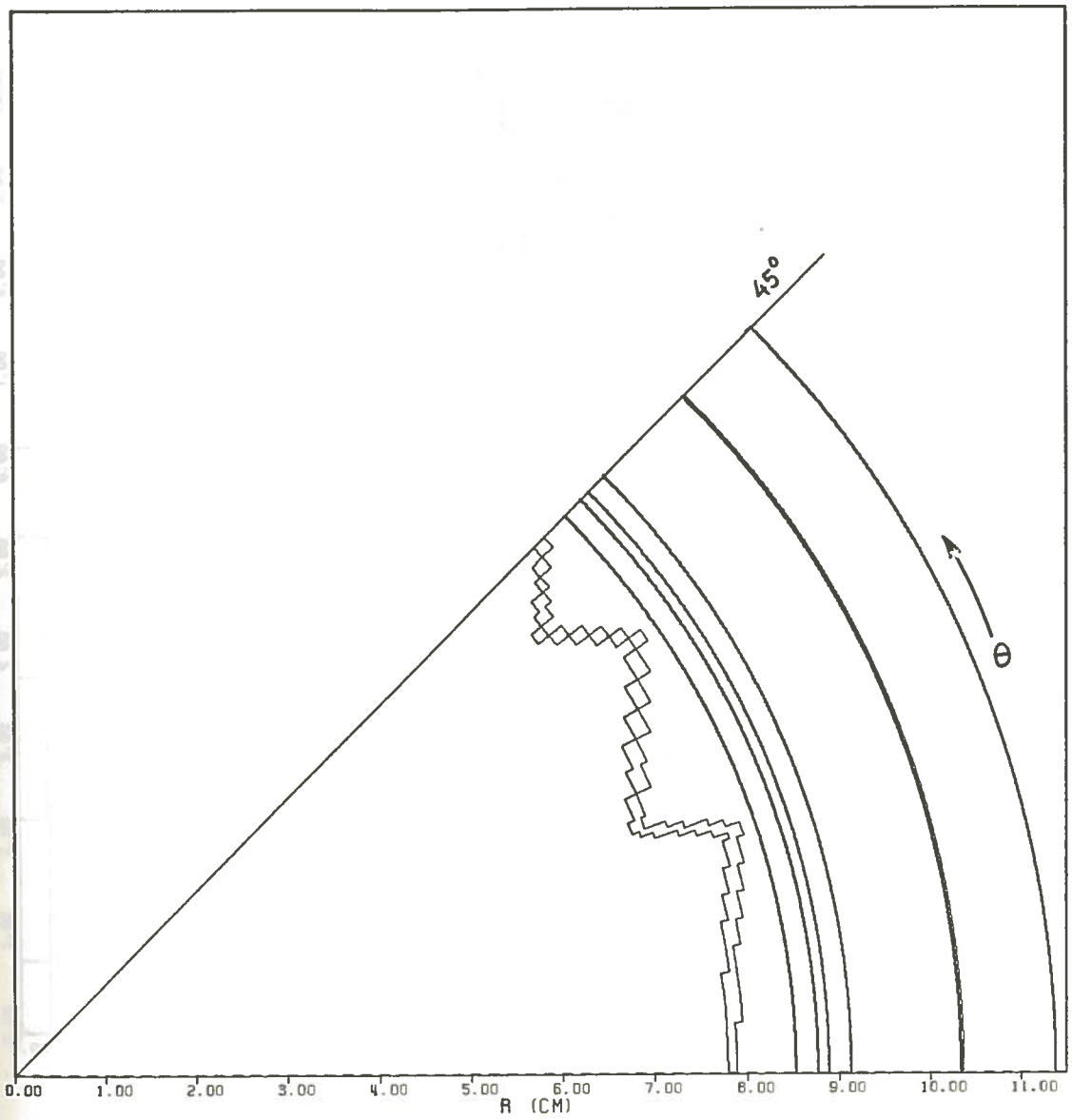

Fig. 15. R-θ representation of 1/8th of the core outer edge of ANO-1 nuclear reactor. scale: 1.0 cm = 21.0 cm

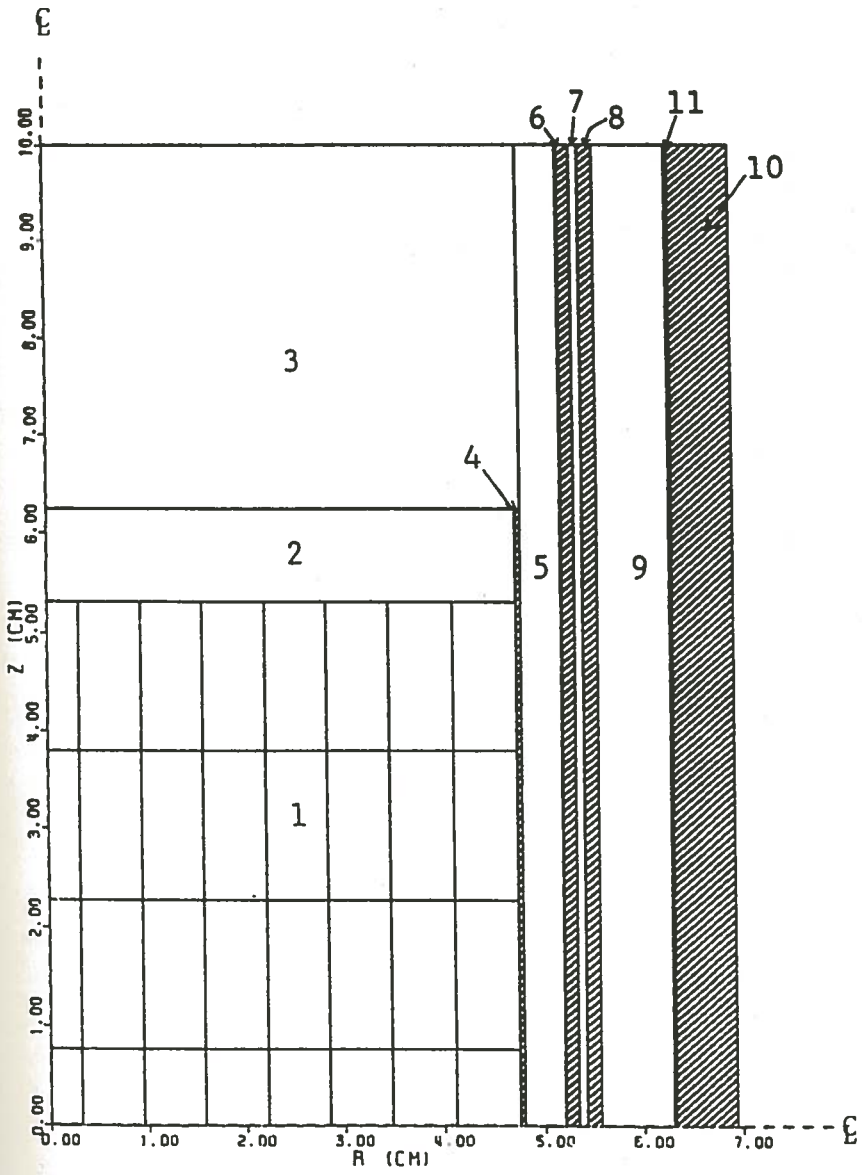

1 - core
2 - upper reflector region
3 - upper reflector steel region
4 - baffle
5 - radial reflector
6 - barrel
7 - water gap
8 - thermal shield
9 - downcomer
10 - RPV
11 - RPV liner

Fig. 16. R-Z view of ANO-1 up to pressure vessel (along R) and nozzle top (along Z). Zones are shown by numbers. scale: 1.0 cm = 34.455 cm

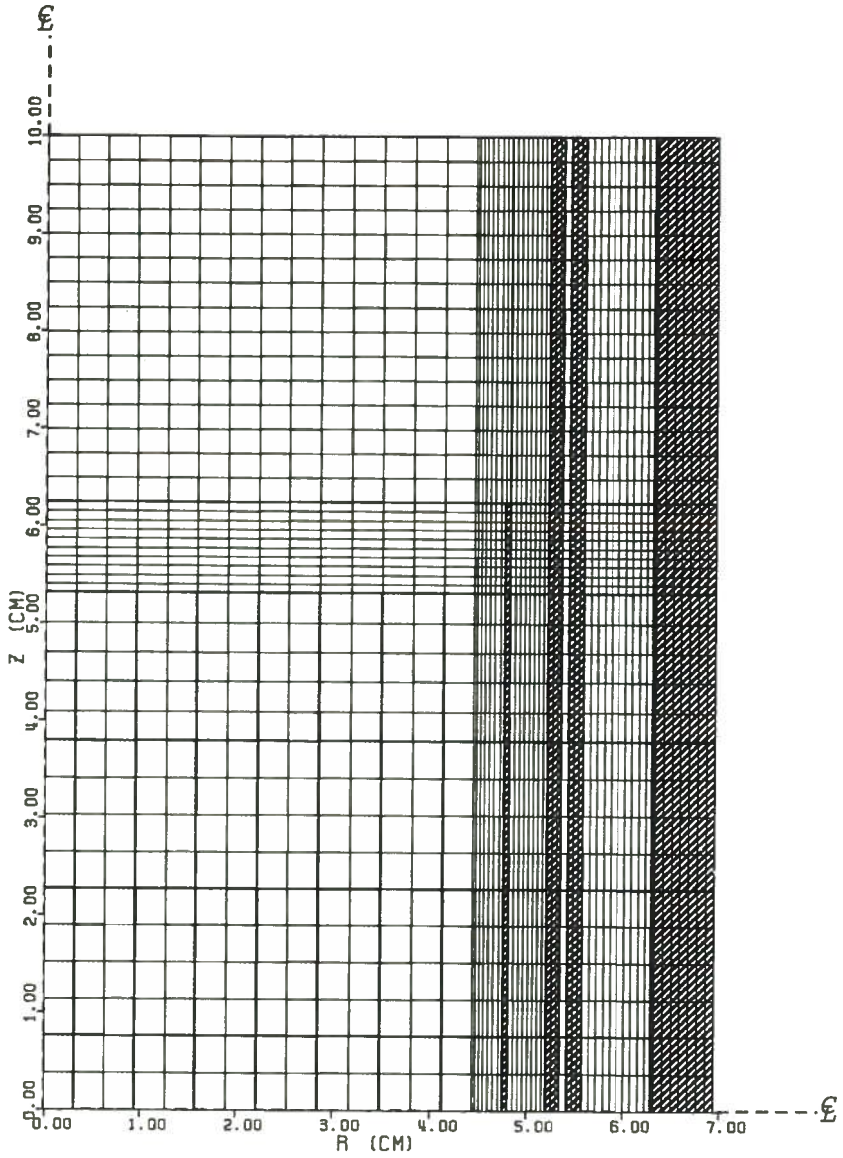

Fig. 17. R-Z model (with meshes) of ANO-1 up to RPV (along R) and nozzle top (along Z) scale: 1.0 cm = 34.455 cm

the normalizations of the R-Z and R sources do not affect the synthesis results, because the respective R-Z and R channel fluxes appear as ratios.

4. The 1-D (R) Model

The DOT-IV 1-D (R) model is shown in fig. 18. Axially, there is only one interval and the number of radial intervals again has been taken to be the same as for the R-θ or R-Z model. The axial mesh is irrelevant, since flow in this direction is not treated in the 1-D calculations. The number of regions in the 1-D model is the same as in the R-θ model (i.e., 9). The 1-D source was obtained by integrating the R-Z source over the Z coordinate to ensure normalization consistency. Input data to DOT-IV for the 1-D calculation are given in Appendix C.

The above three models [R-θ, R-Z, and 1-D (R)] have been used in DOT-IV transport calculations to obtain the channel fluxes for use in the synthesis procedure.

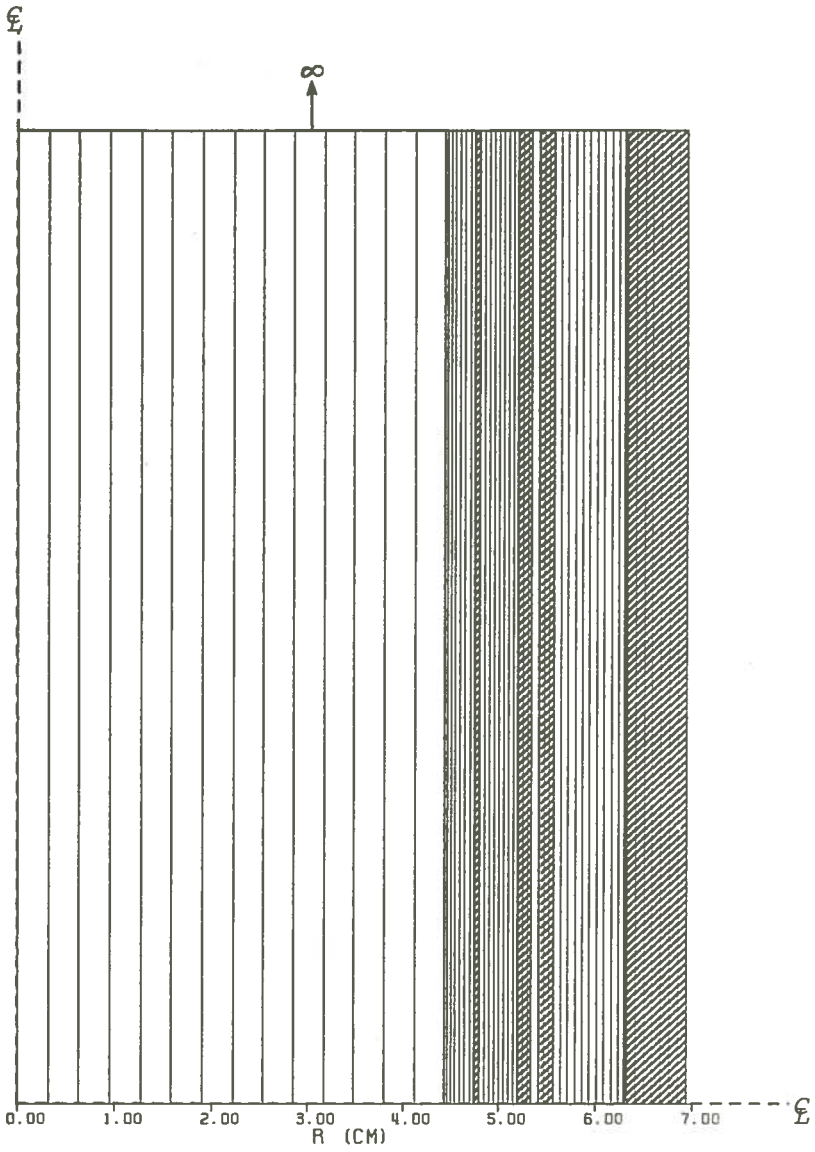

Fig. 18. 1-D model (with meshes) of ANO-1 up to RPV (along R).
scale: 1.0 cm = 34.455 cm

B. Neutron Source Determination for DOT-IV and TORT

The total source in the reactor model has been calculated using a power-to-source conversion factor obtained from the following relation:

$$S_{TOT} = \left[\frac{\nu\Sigma_f}{K\Sigma_f}\right] P \quad - \quad (40)$$

where, $\frac{\nu\Sigma_f}{K\Sigma_f}$ is the power-to-source conversion factor, calculated with the design average burnup[10] (= 29100 MWth-day/ton), and P is the thermal power (= 2599.6 MWth).

The 3-D source distribution was assumed to have the following form:

$$S^{R\theta Z}_{ijk} = Q_{ij} * \mathrm{Cos}(B_z \bar{Z}_k) \quad - \quad (41)$$

$$\text{where } Q_{ij} = \frac{S_{TOT}}{V_{R\theta} \sum_k \mathrm{Cos}(B_z \bar{Z}_k) \Delta Z_k} \quad - - - - - - - - - - - - - - - - - - \quad (42)$$

$V_{R\theta}$ ≡ volume of core region in R-θ geometry;

$\bar{Z}_k$ ≡ axial midpoints for each axial mesh in the core region;

B_z ≡ axial buckling = $\pi/(H+2\delta)$; where, H is the height of active core (= 365.76 cm) and δ is the reflector saving ($\tilde{=}$ 7 cm). The value of B_z is equal to 8.27256E-03 (1/cm).

Equation (41) physically corresponds to a flat source in the R and θ dimensions, and a cosine variation in the Z direction. The source is normalized to an integrated value of

$$S_{TOT} = 2.12614E+20 \text{ (neutron/s)} \quad - - - - - - - - - - - - - - - - \quad (43)$$

The R-θ source is calculated by integrating the R-θ-Z source over the axial dimension as shown below:

$$S_{ij}^{R\theta} = \int_k S_{ijk}^{R\theta Z}\, dk = Q_{ij} \sum_k A_k \Delta Z_k \quad - - - - - - - - - - - - - - - - - - \quad (44)$$

where $A_k = \text{Cos}(B_z \bar{Z}_k)$ and

$\Delta Z_k \equiv$ axial mesh interval.

The R-Z source distribution has a cosine shape and is calculated in the following way:

$$S_{ik}^{RZ} = a * F_i * \text{Cos}(B_z \bar{Z}_k) \quad - \quad (45)$$

where "a" is the appropriate normalization factor; and

$F_i \equiv$ source distribution for all radial mesh points at $\theta = 0°$.

The value of the normalization factor "a" is actually arbitrary as far as the synthesis is concerned. A value of 4.16874E-03 is used in this study so that the total R-Z source and the total R-θ source are consistent with S_{TOT}. For the models used in this study, the R-Z source is four times higher than the R-θ source.

The 1-D source distribution is obtained by summing the R-Z source distribution over the axial dimension as follows:

$$S_i^R = a * F_i * \sum_k \text{Cos}(B_z \bar{Z}_k) \Delta Z_k \quad - - - - - - - - - - - - - - - - - - \quad (46)$$

C. Multigroup Cross Sections Used

The cross-section library SAILOR[11] has been used for nuclear data in the DOT as well as TORT calculations. SAILOR has 47 neutron energy groups and 20 gamma energy groups; however, only the first five out of the 47 neutron energy groups have been used to reduce computing costs for the purpose of this study. Activities have been computed for the following three high-energy threshold dosimeter materials:

$^{59}Co(n,2n)$; $^{58}Ni(n,2n)$; $^{63}Cu(n,\alpha)$.

The threshold energies for the selected dosimeter materials are within the energy boundaries of the five groups.

In performing calculations with DOT-IV and TORT, materials from the SAILOR cross section library have been mixed with a program called GIP (Group-Organized Cross Section Input Program). This has been done in order to get a macroscopic composition comprised of materials from the SAILOR library. In the mixing table, a total of 97 materials from SAILOR have been used to get 29 different compositions for the different material zones and dosimeter materials. In DOT-IV and in TORT, a P_3 Legendre expansion of the scatter cross section has been used. As mentioned earlier, each expansion coefficient is considered a separate material in DOT-IV; but in TORT, a single material is composed of P_0 through P_3 expansions. Hence, we have altogether 8 materials in the TORT calculations.

Materials used in the 3-D and 2-D models, their IDs in the SAILOR cross section library and atom densities are given in tables 2, 3 and 4[10].

TABLE 2

Atom Densities of Fuel* and Corresponding Material IDs in SAILOR Cross Section Library

Material	Atom Density (atom/b-cm)	ID (SAILOR)
U-235	1.541E-04	31 - 34
U-238	6.579E-03	35 - 38
H	2.811E-02	3 - 6
B-10	5.580E-06	7 - 10
O	2.814E-02	39 - 42
Zircaloy-4	4.327E-03	27 - 30
Fe	1.793E-04	19 - 22
Cr	5.299E-04	15 - 18
Ni	2.470E-05	23 - 26

*Atom densities are taken from Batch 6 fuel of ANO-1 tabulated in reference 10 (table 2.6, pp. 2-11).

TABLE 3

Atom Densities* of Materials (other than Fuel) and Corresponding IDs in SAILOR Cross Section Library

Material	Coolant	SS-304	PV-Steel (CS)	ID (SAILOR)
H	4.744E-02			55 - 58
B-10	9.416E-06			7 - 10
O	2.372E-02			59 - 62
Fe		5.978E-02	8.190E-02	131 - 134 (RPV)
				71 - 74**
Cr		1.766E-02	1.270E-04	123 - 126 (RPV)
				63 - 66**
Ni		8.233E-03	4.440E-04	135 - 138 (RPV)
				75 - 78**
C-12		3.222E-04	9.810E-04	139 - 142
				79 - 82†
Mn-55		1.760E-03	1.120E-03	127 - 130
				67 - 70†
Si		1.721E-03	3.710E-04	107 - 110
Al			7.020E-04	103 - 106

*Atom densities are in atom/b-cm

**For materials not in core and RPV

†For materials not in RPV

TABLE 4

Materials and Their Atom Densities in Different Zones of the 3-D and 2-D Models

Zone Name	Materials Composition	Atom Density (atom/b-cm)	Zone (Corresponding to Material) in 3-D	R-Z	R-θ
Core (Fuel)	Same as in Table 2	Same as in Table 2	1	1	1
Baffle	SS-304	Same as in Table 3	2	4	2
Barrel	SS-304	Same as in Table 3	3	6	4
Water Gap	Coolant	Same as in Table 3	4	7	5
Radial Reflector	Coolant	Same as in Table 3	5	5	3
Thermal Shield	SS-304	Same as in Table 3	6	8	6
Downcomer	Coolant	Same as in Table 3	7	9	7
RPV Liner	PV-Steel (CS)	Same as in Table 3	8	11	9
RPV	PV-Steel (CS)	Same as in Table 3	9	10	8
Upper Reflector Region	Zircaloy-4 Coolant Void	4.40419E-04 3.25498E-06	10	2	-
Upper Reflector Steel Region	SS-304 Coolant	0.011752 4.48303E-06	11	3	-

D. DOTSYN Calculations

In performing synthesis with DOTSYN, the computed 1-D (R), R-θ and R-Z scalar fluxes obtained with DOT are used as channel fluxes. The entire radial, azimuthal, and axial ranges are used as the synthesis region. In calculating activities at a given location, the 3-D synthesized group fluxes are first interpolated to the correct axial position. Then a linear interpolation is performed for the azimuthal coordinate. Finally, linear interpolation is performed in the radial direction which gives the desired 3-D group-wise flux at the location specified. The group fluxes are multiplied by the respective reaction cross sections for the desired energy group, and summed over groups to obtain the activity. The input description and input-output requirements for DOTSYN for 3-D flux synthesis are listed in Appendix E. Input data to DOTSYN are listed in Appendix E.1.

CHAPTER IV

RESULTS

Attention was focused primarily on the azimuthal variation of the pressure vessel fluence at three axial locations, namely the midplane, the top of the core and the bottom of the nozzle. These points correspond respectively to the 1st, 15th and 30th axial intervals. It is important for the utilities to routinely monitor fluence at the pressure vessel in order to keep up with the NRC ceiling of maximum allowable fluence for the safe operation of the reactor. The aim of this study is to determine how well and in which locations the synthesis approximation agrees with the exact transport results, and to what extent the synthesis technique is applicable. A comparison of the TORT and DOTSYN group-integrated fluxes (i.e., groups 1 to 5 of SAILOR group structure) computed at the inner surface of the pressure vessel and 1/4T at the peak flux location ($\theta = 9°$) is shown in table 5 and table 6, respectively, for the three axial positions. As seen from these tables, the error in the synthesized flux at this azimuth lies roughly between 0.2% and 3.0% at 1/4T and 0.4% and 5.0% at the inner surface of the pressure vessel. These synthesis results are remarkably good, even at the nozzle elevation. Figures 19, 20 and 21 show the azimuthal variations of the total fluxes at the inner surface of the pressure vessel at the midplane, the top of the core and the bottom of the nozzle, respectively. The synthesis results agree extremely well at the midplane as expected and, as we traverse upward (axially) from the midplane, the

TABLE 5

Comparison of Total Flux by TORT and DOTSYN at the Peak Flux Location (θ = 9°) at the Inner Surface of the Pressure Vessel

Axial Location	TORT	DOTSYN	% Error
Midplane	8.82772E+08	8.79586E+08	0.36
Top of Core	1.38254E+08	1.39760E+08	1.09
Bottom of Nozzle	3.01893E+06	3.16168E+06	4.73

TABLE 6

Comparison of Total Flux by TORT and DOTSYN at the Peak Flux Location (θ = 9°) at the 1/4T of the Pressure Vessel

Axial Location	TORT	DOTSYN	% Error
Midplane	3.96958E+08	3.96089E+08	0.22
Top of Core	6.28489E+07	6.34805E+07	1.00
Bottom of Nozzle	1.35142E+06	1.39600E+06	3.29

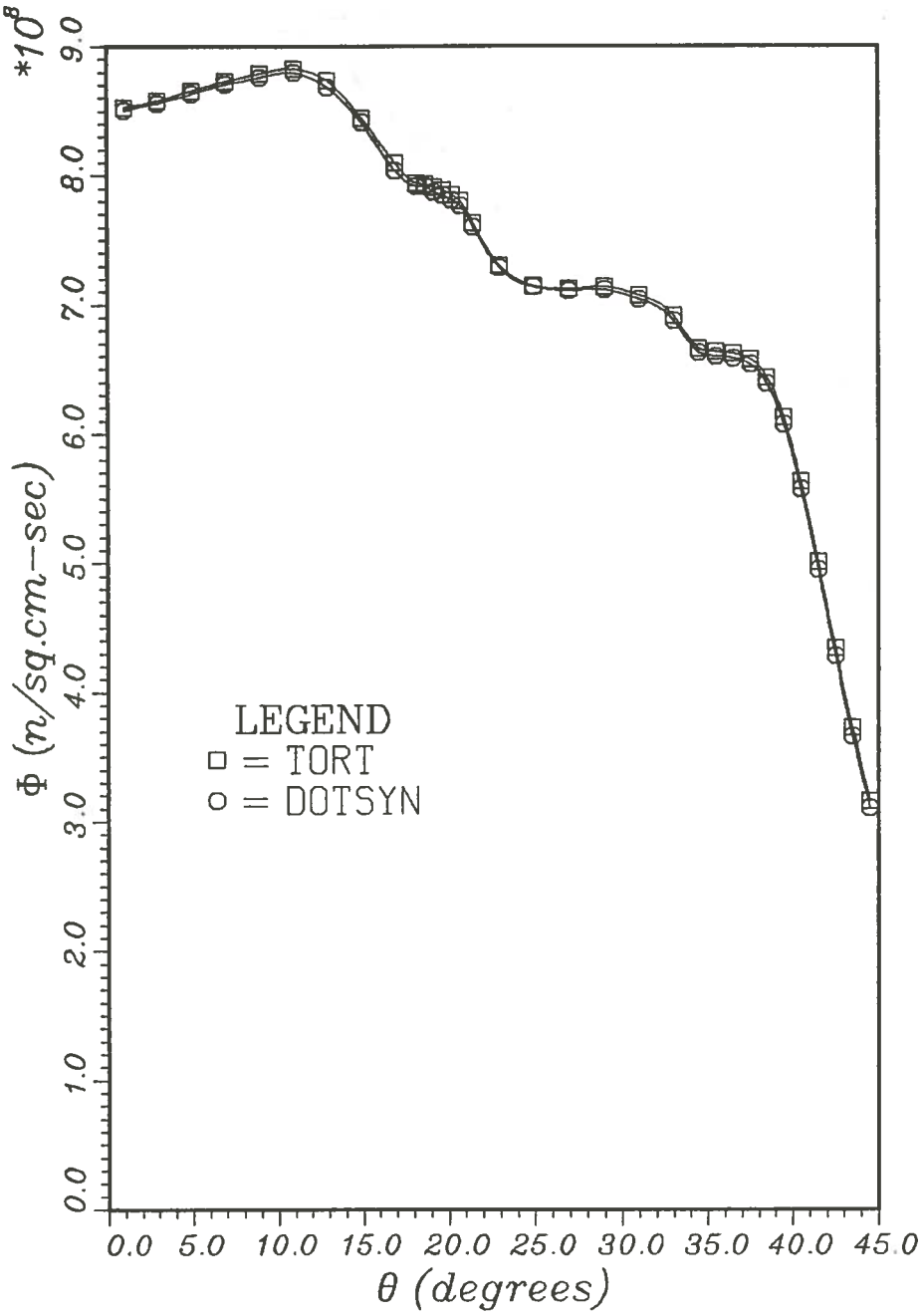

Fig. 19. Azimuthal variation of total flux at the inner surface of RPV. Axial location - midplane

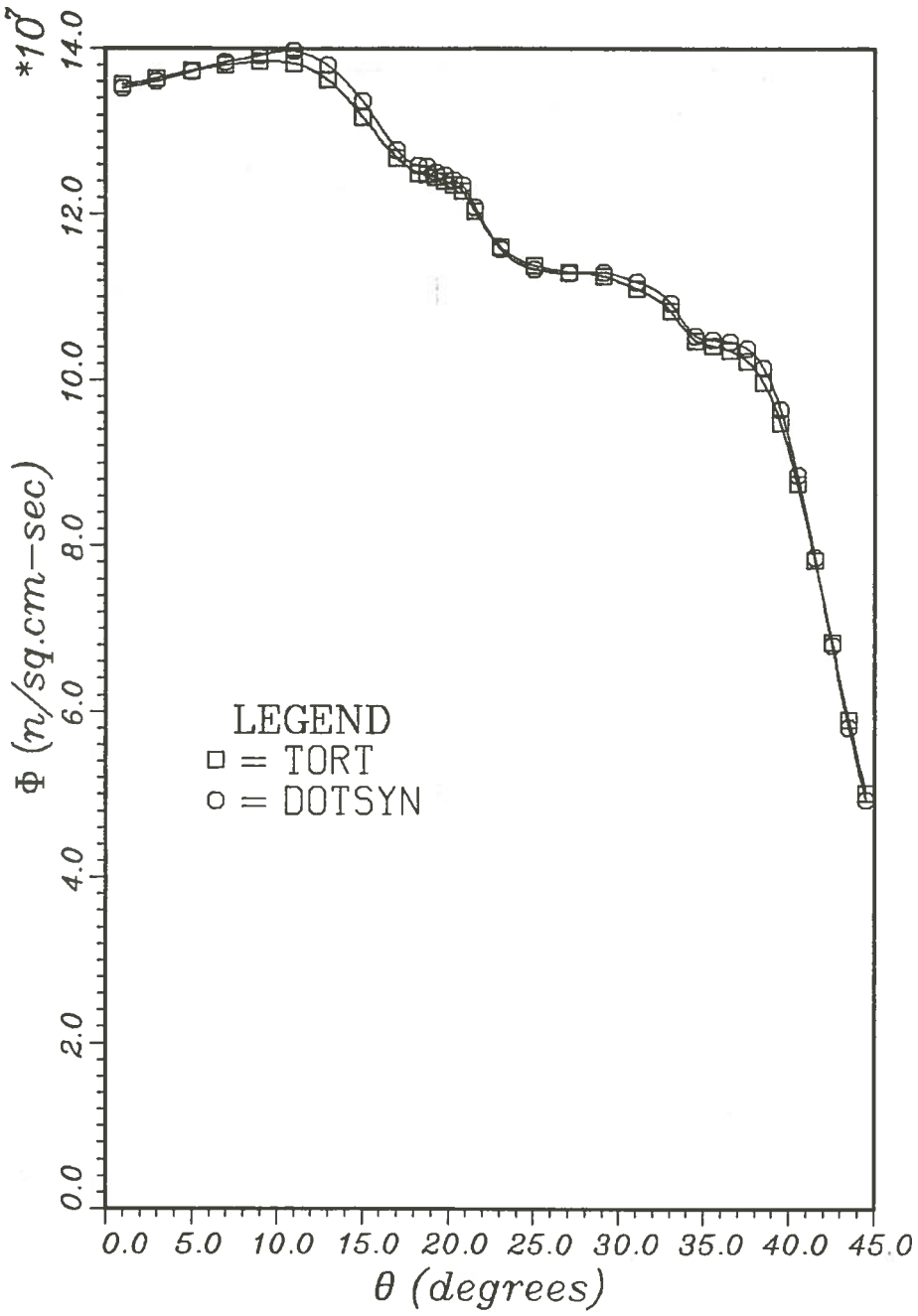

Fig. 20. Azimuthal variation of total flux at the inner surface of RPV. Axial location - top of core

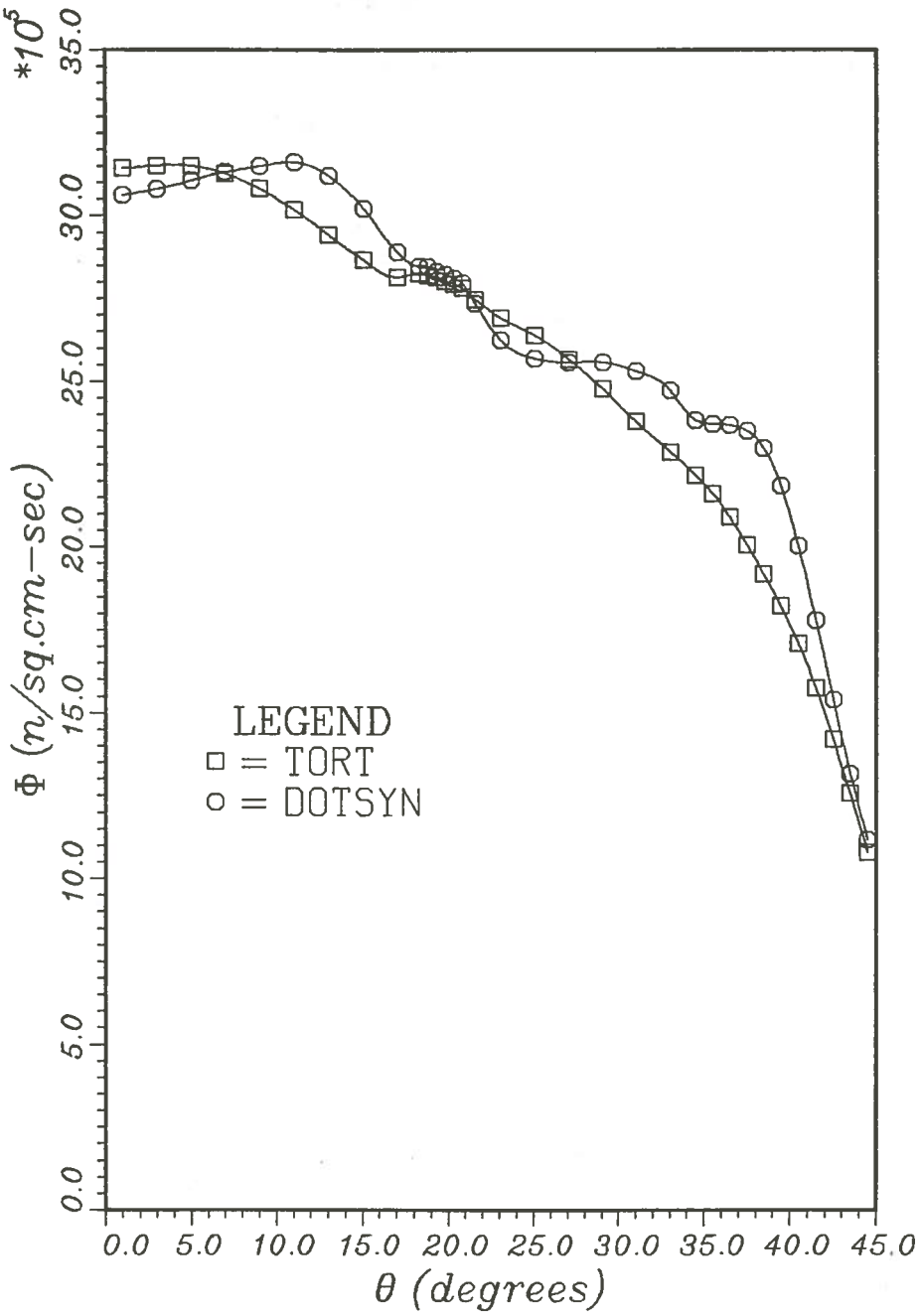

Fig. 21. Azimuthal variation of total flux at the inner surface of RPV. Axial location - bottom of nozzle

results start slowly differing from the TORT results, although they agree very well up to the top of the core. Above the top of the core as we go up further, the shape of the azimuthal flux-variation by TORT slowly smoothes off, whereas DOTSYN retains the same azimuthal shape as at the midplane. This is explained by the fact that in the regions where flux is nearly separable in space (either azimuthally or axially) the 3-D results obtained by DOTSYN are almost exact [see Chapter II, equations (35) and (36)], which accounts for the excellent agreement within the core height. However, DOTSYN does not take care of the flux inseparability wherever it occurs, whereas TORT does; i.e., in DOTSYN the shape of the flux variation obtained at the midplane is retained everywhere. Up to the top of the core, the flux is separable in space so that all Z levels have nearly the same flux shape in the R-θ coordinates. Above the core, the R-θ variation is no longer separable in Z, and as we move up (axially) the characteristic R-θ variation changes. From figure 21, it is seen that the typical R-θ shape of the azimuthal distribution of flux within the core height "smoothes off" above the core region, and a more uniform azimuthal variation is obtained. The characteristic shape of the azimuthal flux variation at the midplane and the top of the core is due to the shape of the core and the source distribution accordingly. The azimuthal shape of the flux above the core is more uniformly distributed and, because of the void boundary condition at the 45° slice, the magnitude of flux falls off as we move from 0° to 45° angle. At the bottom of the nozzle, the divergence of the DOTSYN values from the TORT ones is maximum as we expect, but as shown in Chapter II by the equations (37) and (38), the synthesis approximation used in DOTSYN [equation (34)] still preserves the

integrated or the average values of the flux in the azimuthal coordinate at any radial location R. The average flux calculated, respectively, with TORT and DOTSYN at the bottom of the nozzle is equal to

$$\phi^{TORT}_{ave} = 2.46015E+06; \quad \phi^{DOTSYN}_{ave} = 2.55883E+06$$

These values agree within 4.0%.

Group-wise activities were calculated at the bottom of the nozzle and the inner surface of the pressure vessel for $^{59}Co(n,2n)$, $^{58}Ni(n,2n)$ and $^{63}Cu(n,\alpha)$ and then they were summed over groups; the azimuthal variation of these activities is illustrated in figures 22, 23 and 24, respectively. The first five energy groups from the SAILOR cross section library vary between 17.33 MeV and 7.408 MeV. The variation of the group fluxes per MeV for these energy groups are shown in figures 25, 26 and 27 which correspond to the midplane, the top of the core and the bottom of the nozzle, respectively. The 5-group flux spectrum predicted by DOTSYN agrees extremely well with the TORT results at the midplane and the top of the core for the same reasons explained above. At the midplane, there is virtually no difference between DOTSYN and TORT results. At the top of the core, DOTSYN flux spectrum disagrees with the TORT flux spectrum by a maximum of 1.17% in the lower energy groups; and at the bottom of the nozzle, the maximum disagreement between these two calculations lies within 4.0%, which shows that the much less expensive synthesis method of 3-D flux estimation produces very reasonable and acceptable results compared to TORT.

Figures 28 and 29 show the radial variation of the total flux at the peak flux location ($\theta = 9°$), at the midplane and the top of the core. As predicted and shown theoretically (Chapter II), in the regions where

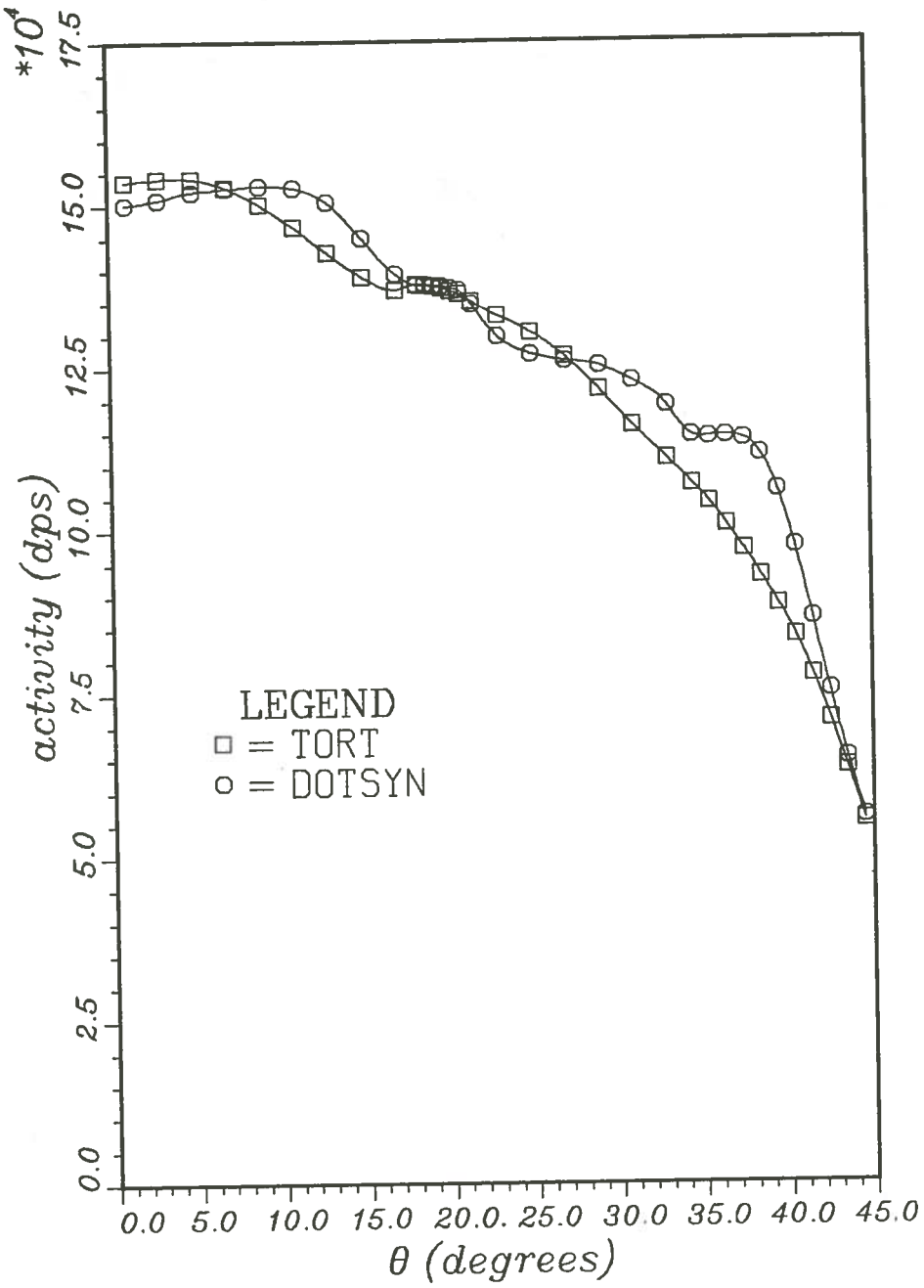

Fig. 22. Azimuthal variation of total activity for Co-59(n,2n) at the inner surface of RPV. Axial location - bottom of nozzle

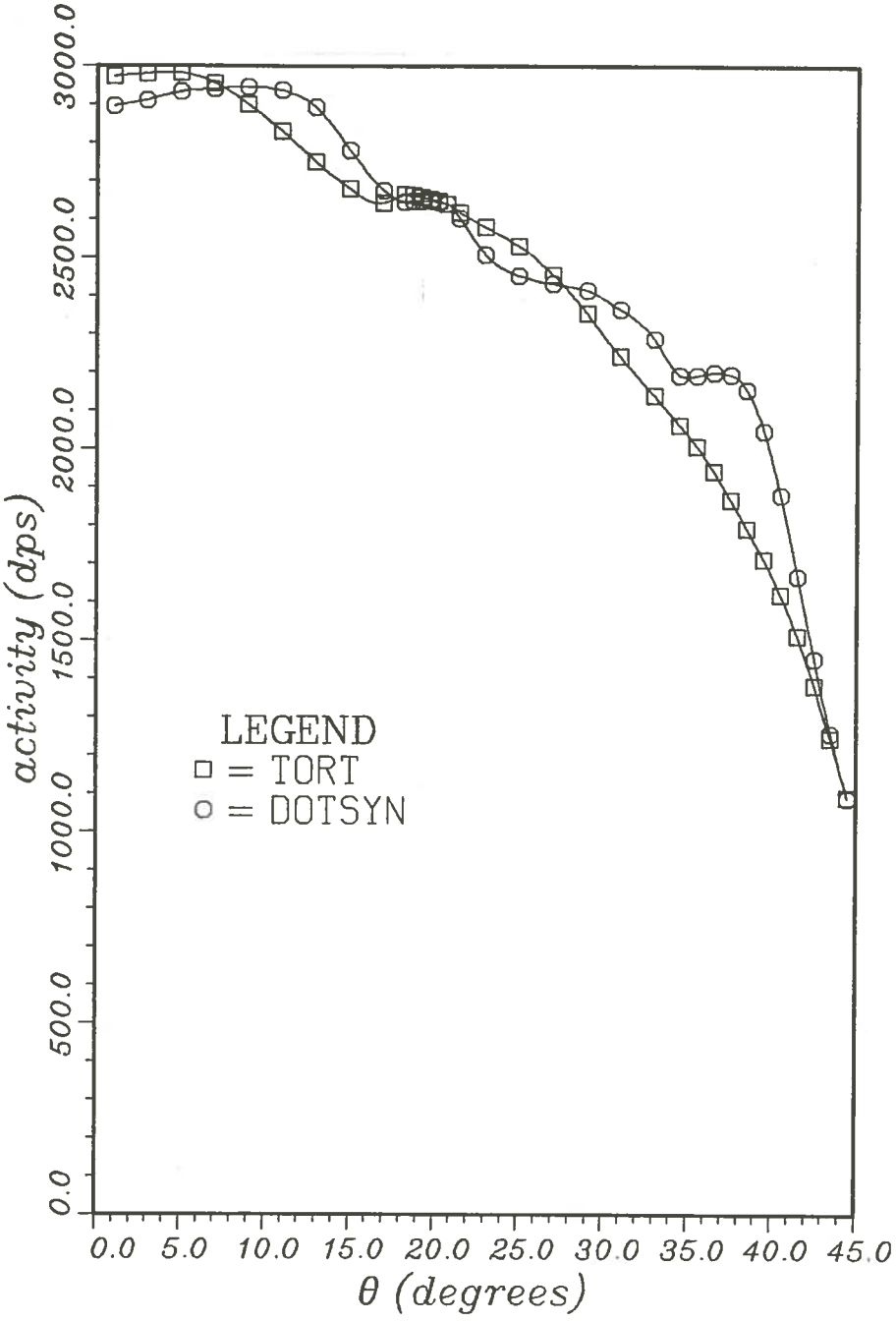

Fig. 23. Azimuthal variation of total activity for Ni-58(n,2n) at the inner surface of RPV. Axial location - bottom of nozzle

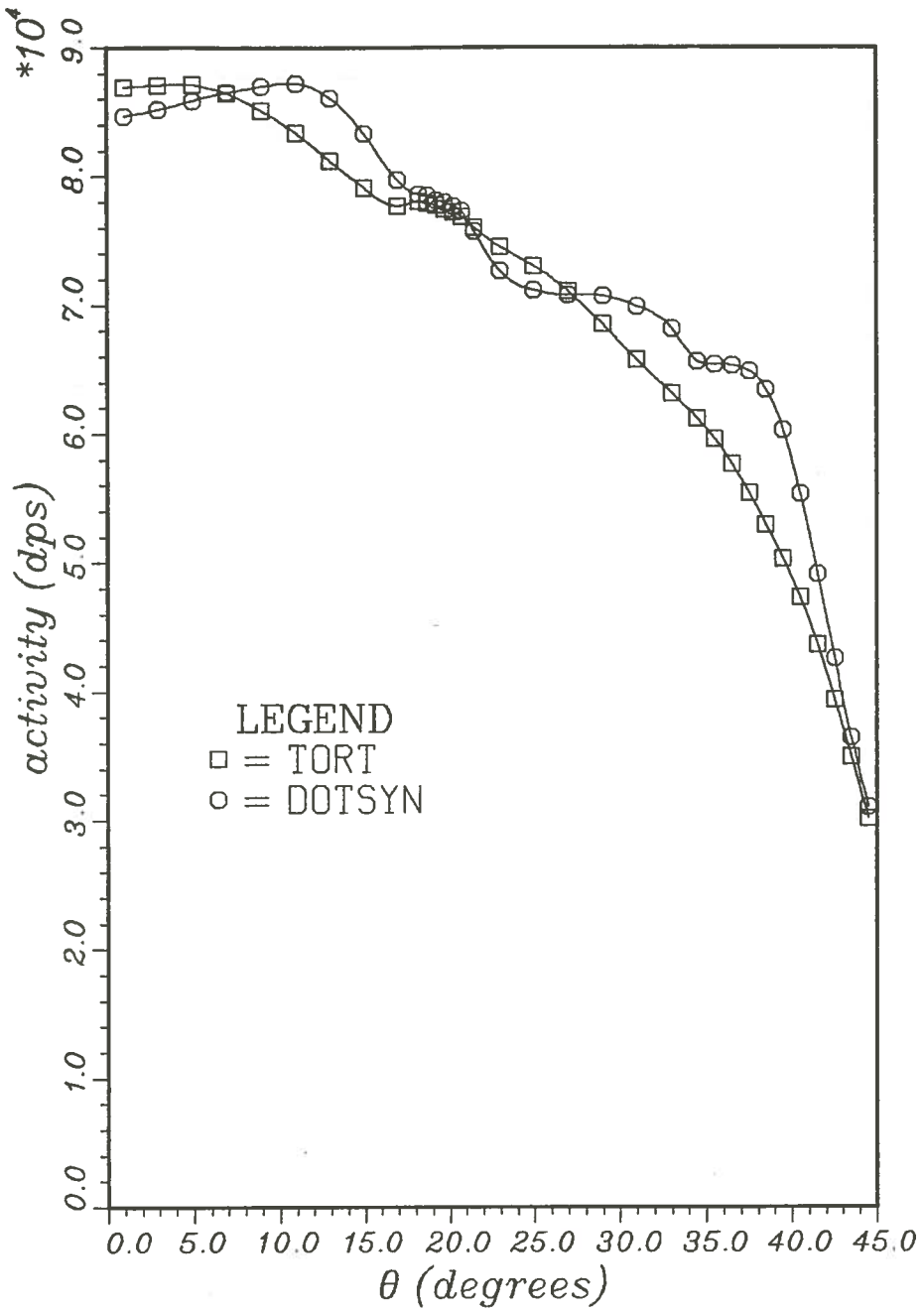

Fig. 24. Azimuthal variation of total activity for Cu-63(n,α) at the inner surface of RPV. Axial location - bottom of nozzle

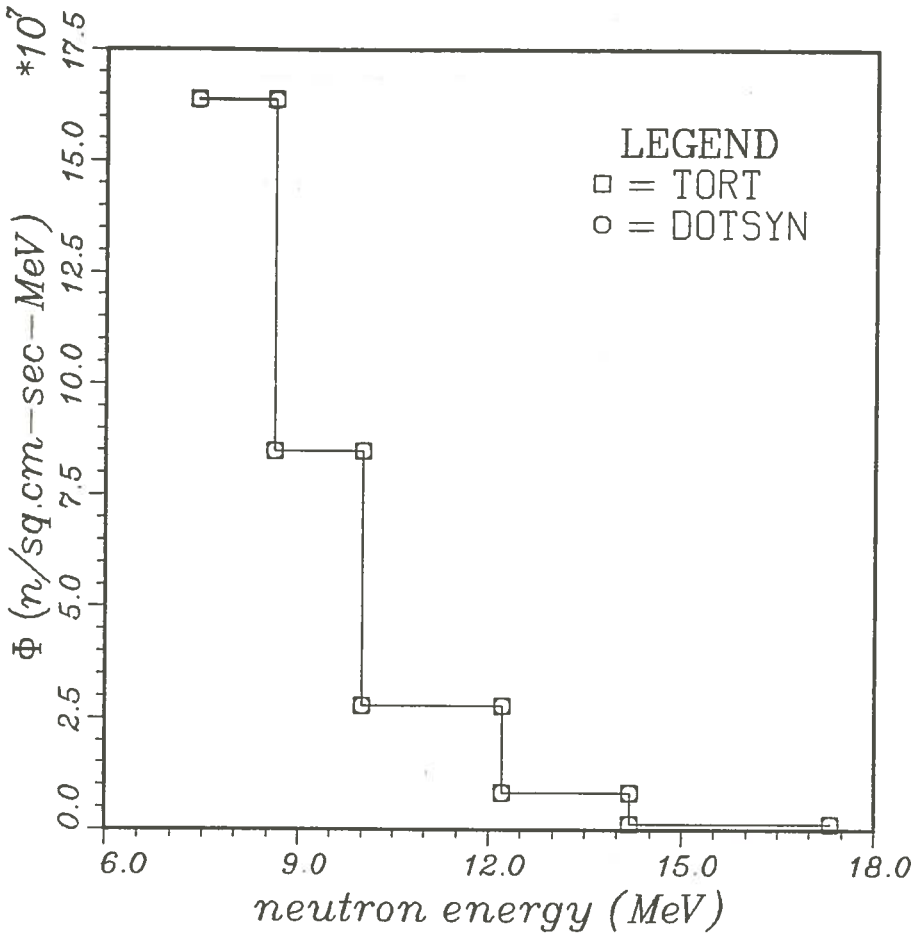

Fig. 25. Neutron energy spectrum at the RPV inner surface at the peak flux location (θ = 9°). Axial location - midplane

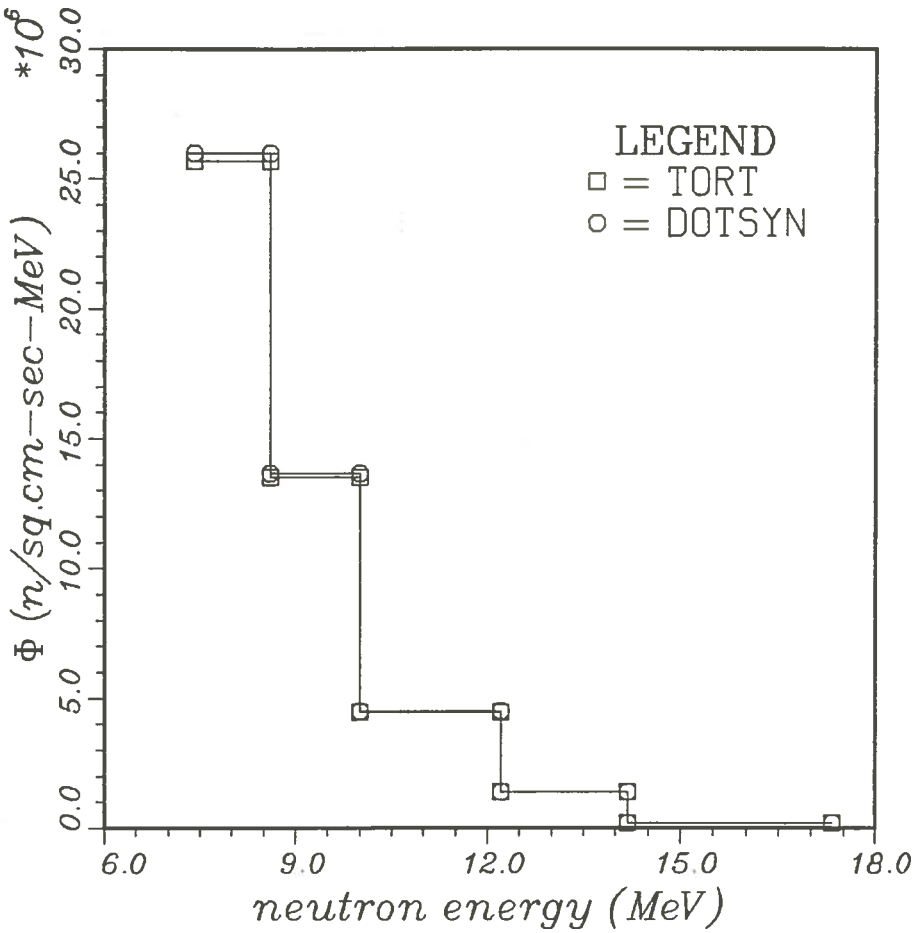

Fig. 26. Neutron energy spectrum at the RPV inner surface at the peak flux location (θ = 9°). Axial location - top of core

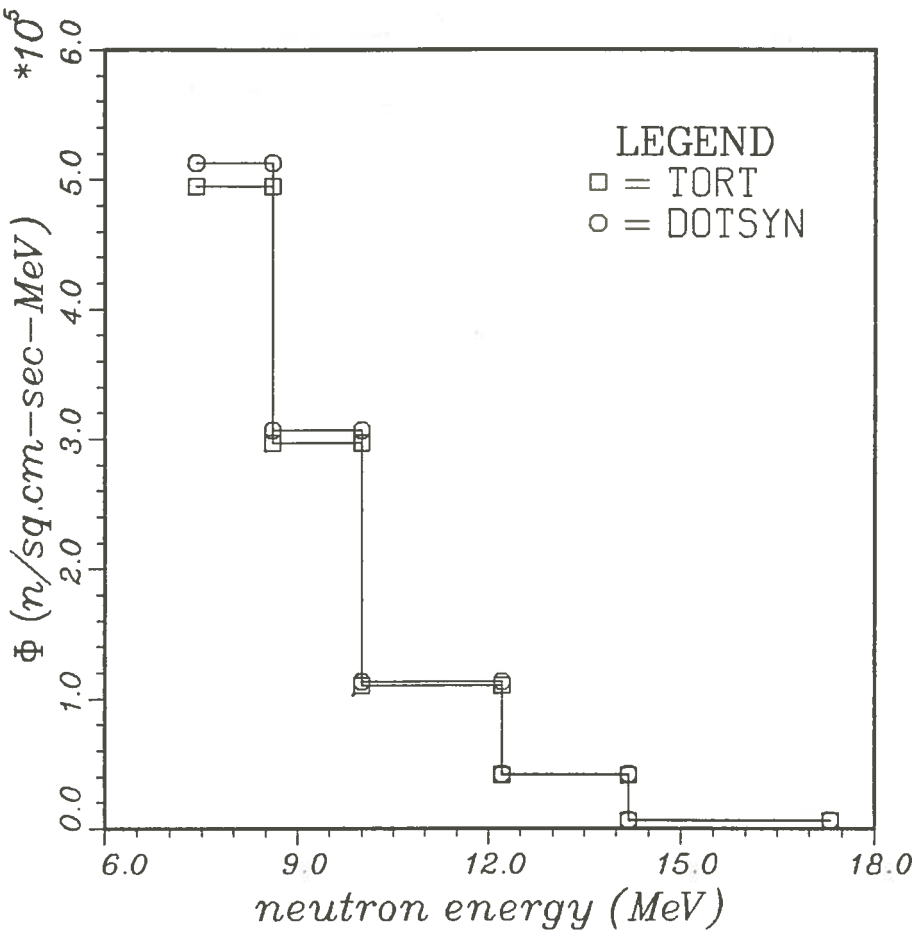

Fig. 27. Neutron energy spectrum at the RPV inner surface at the peak flux location (θ = 9°). Axial location - bottom of nozzle

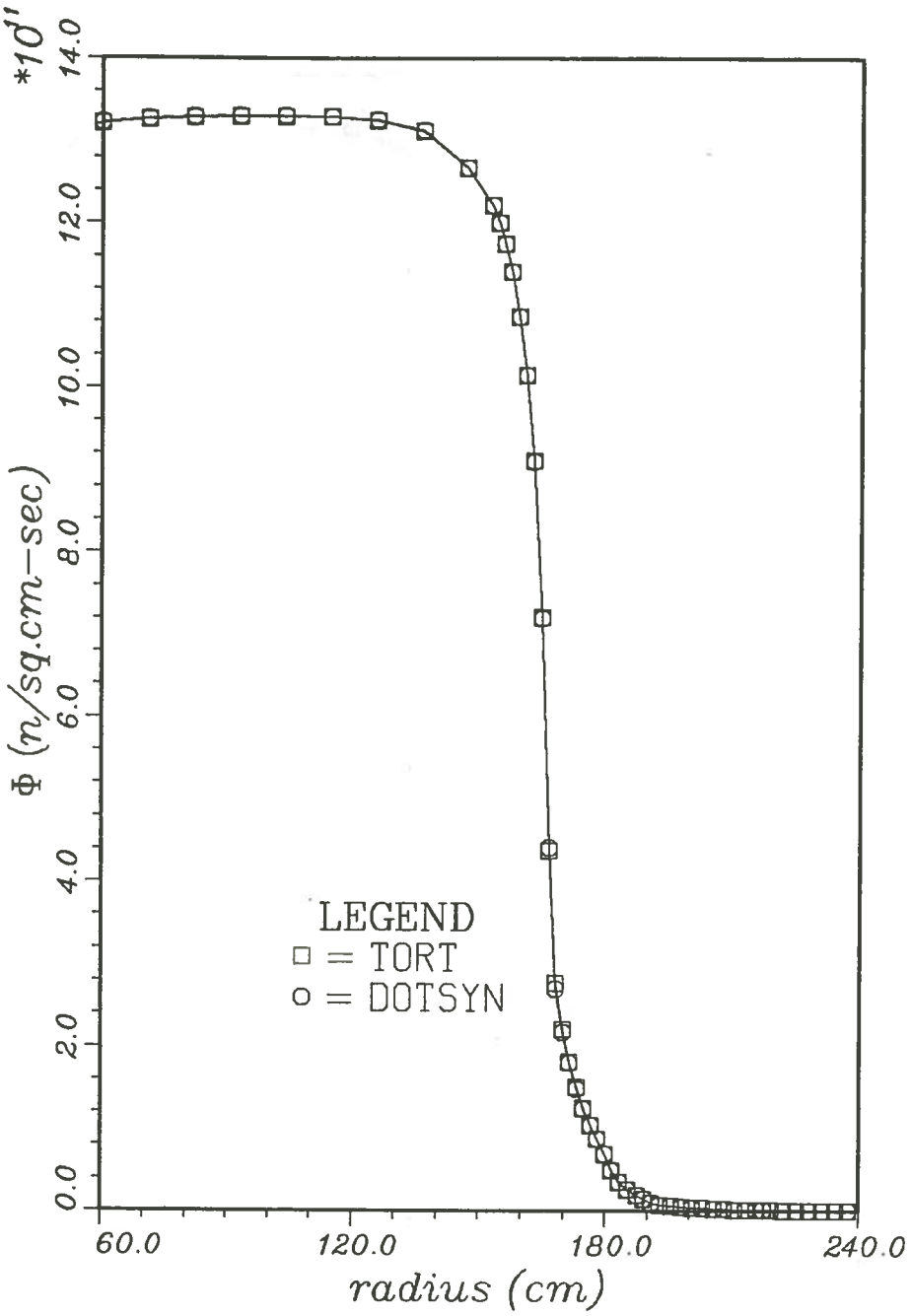

Fig. 28. Radial variation of total flux at the peak flux location (θ = 9°). Axial location - midplane

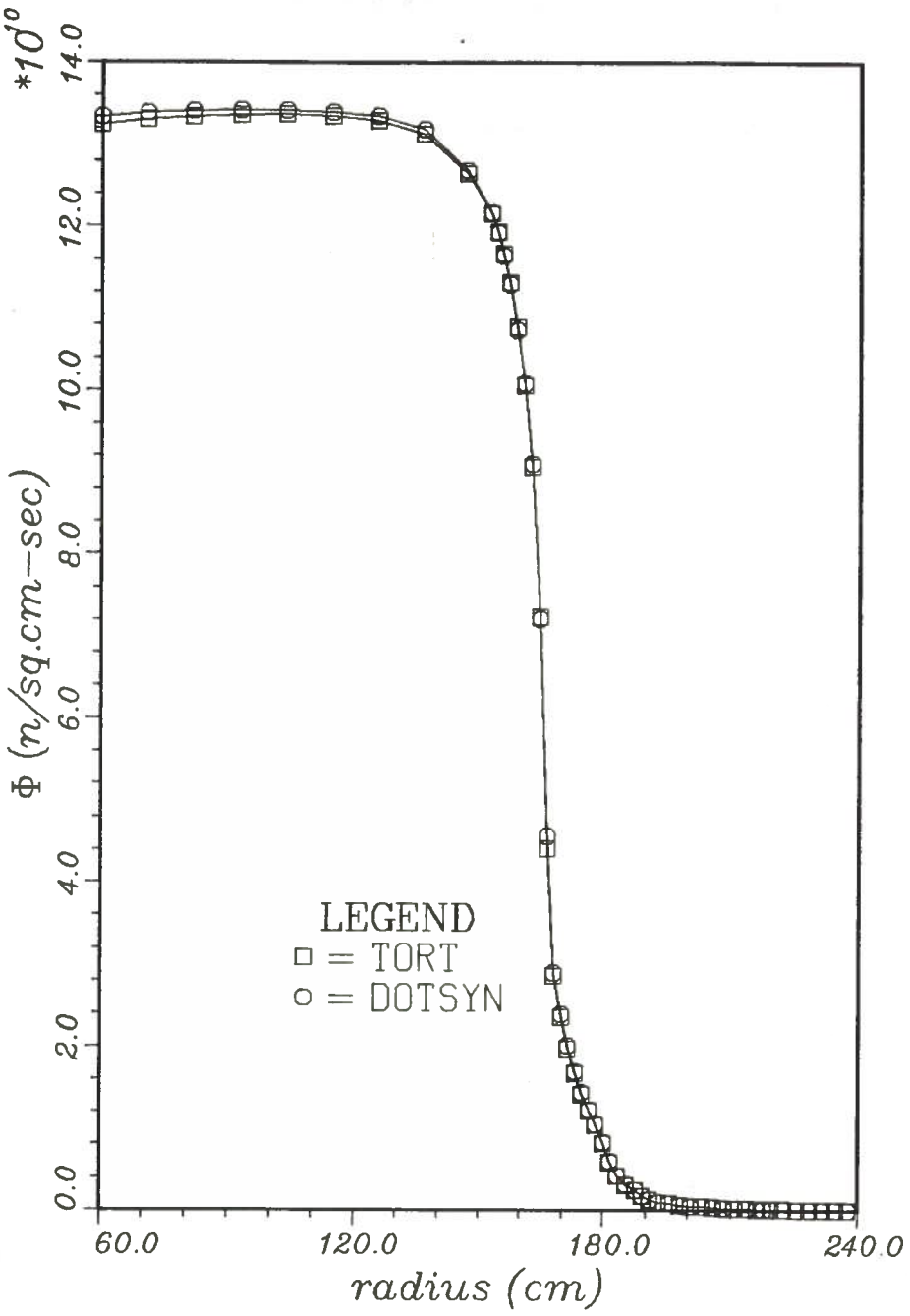

Fig. 29. Radial variation of total flux at the peak flux location (θ = 9°). Axial location - top of core

flux is nearly separable such as the midplane, the synthesis expression for flux is almost exact compared to the true 3-D flux distribution. At the top of the core, there is also very little disagreement between DOTSYN and TORT calculations (within 0.7%). As seen from these two plots, at two important locations - directly in front of the pressure vessel and at the 1/4T - the fluence predicted by DOTSYN is very accurate compared to TORT.

Figure 30 illustrates the radial variation of the total flux at the peak flux location ($\theta = 9°$) and at the bottom of the nozzle. As seen in this figure, the flux shape behaves strangely starting from a certain radial location. This location corresponds to the 15th radial interval which starts roughly at 152.0 cm. At this location, the flux values suddenly jump up, then dip down, and finally making another jump, fall down rapidly. Near the core region, this behavior is not observed; but as we go up further, the situation gradually worsens. This behavior is predicted by TORT as well as DOTSYN. It was found from the calculations that, in the case of the synthesis, only the R-Z channel flux shows these oscillations which start approximately at the 28th axial interval. This interval belongs to zone 3 (fig. 16) - the upper reflector steel region - which contains a mixture of SS-304 and coolant, the latter having a density of about 0.7. Axially, there are 10 equal intervals in zone 2 which are narrower than the ones in zone 3 which has 15 equal intervals.

Two test runs were performed in order to see the effect of width of the axial intervals on the flux shape. In the first test run, the 25 intervals above the core are kept equally spaced (axially) each having a width of about 6.5 cm and the second test run contained only 16 equally

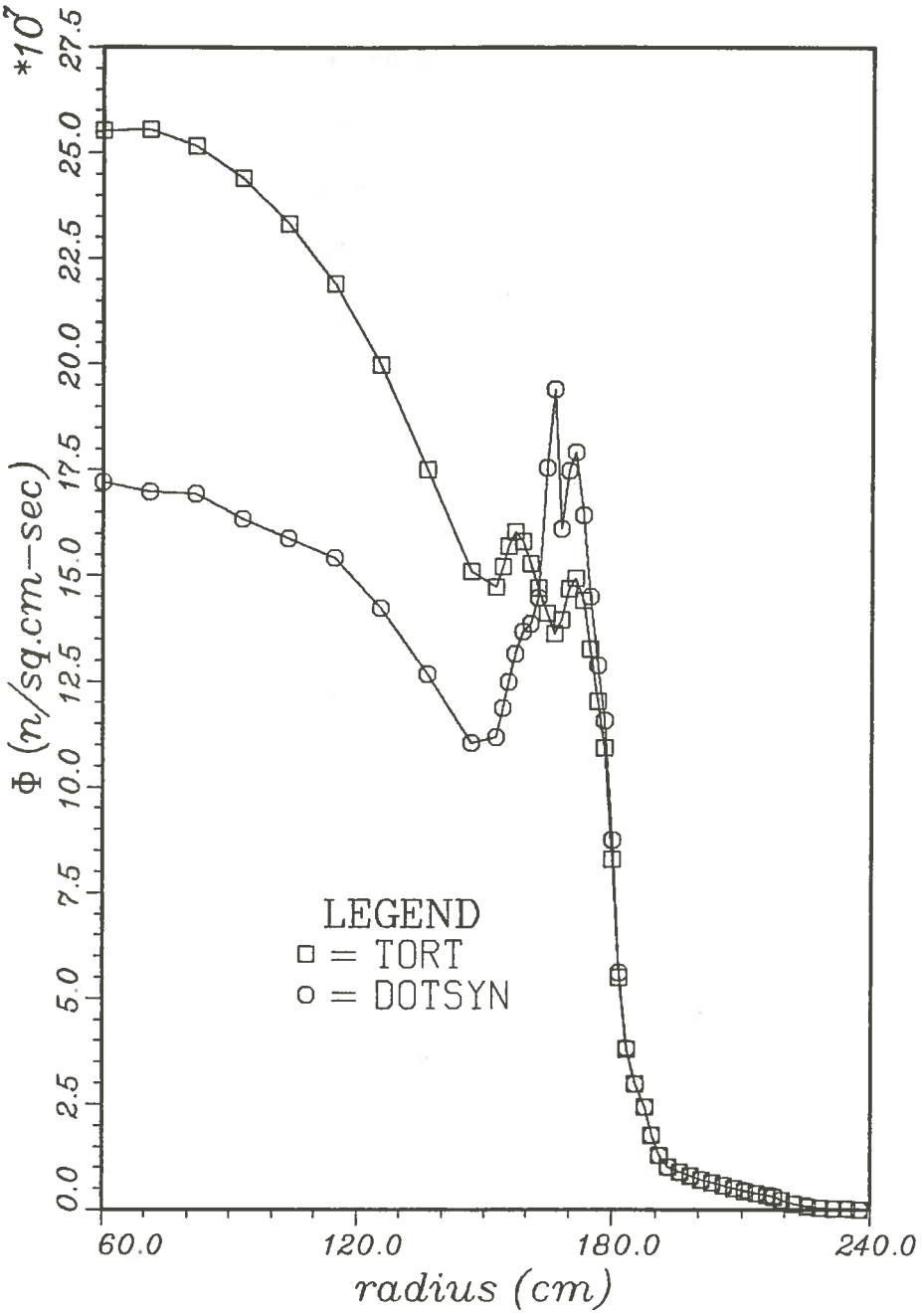

Fig. 30. Radial variation of total flux at the peak flux location (θ = 9°). Axial location - bottom of nozzle

spaced axial intervals above the core, each of which is about 10.0 cm wide comparable to the 10.45 cm width at the upper part of the core. In both test runs, the oscillations persist. The first 14 radial intervals in the core are equally spaced, and they are about seven times wider than the 7 intervals starting from the 15th. It is the 15th radial interval also where the flux values start oscillating - thus the behavior may be caused by the sudden change in the width of the radial intervals. This is a problem associated with the numerical method applied in the DOT R-Z as well as TORT calculations. TORT applies only the weighted difference and, hence, the same method was adopted with DOT.

Finally, two more tests were performed with 21 equally spaced (about 7.9 cm wide) radial intervals in the core. In the first of these two tests, the number of Z intervals is kept the same as in the very initial run and in the second test, the Z intervals are equally spaced above the core. In both the cases, it is found that the radial location of the flux oscillations now shifts to where the narrower mesh starts, i.e., now the oscillations start not at the 15th but at the 22nd radial interval (location of the relatively narrow meshes). The axial location of these oscillations did not vary noticeably.

It can be concluded from the above information that in performing the R-Z calculations, flux oscillations can be expected at the locations where the radial meshes are very narrow compared to the axial meshes. This is basically because of the fact that a neutron has to travel a long way axially in order to traverse radially from one side of the interval to the other. This sometimes produces negative flux which eventually results in an oscillatory behavior of the flux shape. This is not seen in the core region because of the source neutrons generated within the interval.

Notice from figure 30 that at the locations of concern - in front of the pressure vessel (R = 217.17 cm) and at 1/4T (R = 222.00 cm) - the oscillations have no effect, and DOTSYN virtually gives the same values as TORT in predicting the fluence.

It is to be noted from the above tests that in performing these calculations it is a good idea to use meshes which are close to squares; in other words, avoid long, narrow intervals in the transport computations.

CHAPTER V

SUMMARY AND CONCLUSIONS

In this study, a three-dimensional flux synthesis program called DOTSYN has been developed for use in reactor pressure vessel fluence calculations in power reactors. The method is based on combining 2-D R-θ and R-Z DOT transport calculations to obtain an R-θ-Z (synthesized) flux distribution. The accuracy has been established by comparison with 3-D discrete ordinates calculations performed with the code TORT. Results indicate that the synthesis approximation developed in this study produces extremely good results for threshold activities in the RPV. At axial locations within the core region, the agreement is virtually exact. Above the core, the error is within 5% at the peak flux location and in the worst case, at the nozzle level, the maximum error is within 20%. The latter location is 61.67 cm from the core top. The five-group flux spectrum predicted by DOTSYN agrees extremely well with that by TORT. At the midplane, there is virtually no disagreement. At the top of the core, the disagreement is within 1.17% and that at the bottom of the nozzle lies within 4.0%. Although in some cases, the disagreement between DOTSYN and TORT reaches about 20.0%, the computer time (actual CPU time) required by DOTSYN (plus the 2-D DOT calculations) is about 35 times less than that required by TORT for a model such as the one used in this study. This is a very important consideration for the utilities who routinely calculate neutron flux in the power reactors. Hence, the synthesis approximation is quite efficient and economical and can be

used for routine reactor fluence calculations with a maximum estimated error of about 20% at locations far above the top of the core.

Several extensions to the present study are recommended. First, the accuracy of the synthesis approximation for lower energy groups needs to be established. Also, the accuracy has not been determined for more complex source distributions (such as for "part-length shield assembly" cores). Currently, DOTSYN is not applicable to all geometries. In this study, the cylindrical geometry (R-θ-Z) has been treated. The code has not yet been tested for an X-Y-Z geometry. It is possible to transform DOTSYN to a more general synthesis code. For example, DOTSYN does not treat a variable mesh within the synthesis region; this restriction can be overcome. In the activity calculation subroutine, there is an option to collapse 56 energy groups to any lower number of groups and this is valid only for the ELXSIR cross section library. This option can be extended to cover other cross section libraries as well, such as SAILOR used in this study.

REFERENCES

1. R. E. Maerker, M. L. Williams and B. L. Broadhead. "Summary Documentation of EPRI Workshop on LWR Pressure Vessel Fluence Calculations with LEPRICON Code System". Meeting, held at Palo Alto, California; April 18-19, 1983.

2. S. Kaplan. "Some New Methods of Flux Synthesis", Nuclear Science and Engineering; 13: 22-31; 1962.

3. A. F. Henry. Nuclear Reactor Analysis. The MIT Press, Cambridge, Massachusetts, and London, England; 1975.

4. Nobuo Sasamoto and Kiyoshi Takeuchi. "Direct Integration Method for Solving the Neutron Transport Equation in Three-Dimensional Geometry", Nuclear Science and Engineering; 80: 554-569; 1982.

5. R. Sanchez and N. J. McCormick. "A Review of Neutron Transport Approximations", Nuclear Science and Engineering; 80: 481-535; 1982.

6. E. E. Lewis and W. F. Miller, Jr. Computational Methods of Neutron Transport. John Wiley and Sons Inc., New York; 1984.

7. Weston M. Stacey, Jr. Variational Methods in Nuclear Reactor Physics. Academic Press, New York and London; 1974.

8. M. L. Williams, P. Chowdhury and B. L. Broadhead. "DOTSYN: LEPRICON Module for Synthesizing 3-D R-θ-Z Flux Distribution". Electric Power Research Institute, Palo Alto, California; (in press).

9. R. E. Maerker, B. L. Broadhead, Chia-Yao Fu, Jehudah Wagschal, John Williams and M. L. Williams. "Combining Integral and Differential Dosimetry Data in an Unfolding Procedure with Application to the Arkansas Nuclear One-Unit 1 Reactor".

10. "Calculation of Neutron Energy Spectra in the Core and Cavity of a PWR (ANO-1)". Topical Report, NP-3776. Electric Power Research Institute, Palo Alto, California; December, 1984.

11. G. L. Simmons and R. Roussin. "RSIC Data Library Collection (DLC - 76) - SAILOR - Coupled, Self-shielded, 47 Neutron, 20 Gamma-Ray, P_3, Cross Section Library for Light Water Reactors". Radiation Shielding Information Center, Oak Ridge, Tennessee.

VITA

Prosanta Chowdhury was born on the 28th of December 1951 in Gaibandha, Bangladesh. He received his primary, secondary and higher secondary education in Gaibandha, Bangladesh, and B.S. and M.S. (combined) (with Honors) in Electrical Engineering from Moscow Power Engineering Institute, Moscow, USSR, in 1982, specializing in Power Stations, Transmission and Distribution, Network and Systems. After his M.S. in Electrical Engineering, he worked for 14 months as Office Engineer in a private company in Dhaka, Bangladesh, dealing with the extension of an existing 110 MW thermal power plant by two 220 MW units. He was admitted to the Nuclear Engineering curriculum in the Nuclear Science Center of the Louisiana State University in January 1984, and received his M.S. in Nuclear Engineering in May 1987.